Dystrophic *mdx* mouse myoblasts exhibit elevated ATP/UTP-evoked metabotropic purinergic responses and alterations in calcium signalling.

Justyna Róg[1,4], Aleksandra Oksiejuk[1], Maxime Gosselin,[2] Wojciech Brutkowski[1], Dorota Dymkowska[1], Natalia Nowak[3], Samuel Robson,[2] Dariusz C. Górecki[2,4*] Krzysztof Zabłocki[1*+]

[1] Laboratory of Cellular Metabolism, Nencki Institute of Experimental Biology of the Polish Academy of Sciences, 3 Pasteur Str., 02-093 Warsaw, Poland

[2] School of Pharmacy and Biomedical Sciences; University of Portsmouth; Portsmouth, UK

[3] Laboratory of Imaging Tissue Structure and Function, Neurobiology Center Nencki Institute of Experimental Biology of the Polish Academy of Sciences, 3 Pasteur Street 02-093 Warsaw, Poland

[4] Military Institute of Hygiene and Epidemiology, Warsaw, Poland

[*] senior co-authors (equal contribution)

[+] Corresponding author: K. Zabłocki, Nencki Institute of Experimental Biology, 3 Pasteura str. 02-093 Warsaw, Poland; e-mail: k.zablocki@nencki.gov.pl

Key words: calcium signalling, muscular dystrophy, myoblasts, purinergic receptors

Running title: *mdx* mutation affects calcium signalling in myoblasts

Highlights:

1. NGS reveals changes in Ca^{2+} signalling-related RNAs in mdx myoblasts

2. *Mdx* myoblasts exerts increased susceptibility to P2RY2-mediated stimulation

3. Levels of several Ca^{2+} signalling-related proteins are changed in *mdx* myoblasts

4. P2RY2 agonist slows-down *mdx* myoblasts motility

Abbreviations: $[Ca^{2+}]c$, cytosolic Ca^{2+} concentration; DMD, Duchenne Muscle Dystrophy; NCX, sodium-calcium exchanger; PLC, phospholipase C, PMCA, plasma membrane calcium ATP-ase; SERCA, sarco-endoplasmic reticulum calcium ATP-ase;

Acknowledgements

This work was supported by the National Science Centre, Poland accordingly to the decision number DEC-2013/11/B/NZ3/01573.
The research was performed in part in the Multimodal Laboratory of Cell Adhesion and Motility, part of NanoFun laboratory co-financed by the European Regional Development Fund within the Innovation Economy Operational Programme POIG.02.02.00-00-025/09.

Summary

Pathophysiology of Duchenne Muscular Dystrophy is still elusive. Although progressive damage to muscle fibres is a cause of muscle deterioration leading to premature death, there is a growing body of evidence indicating that the triggering effects of DMD mutation are present at the very early stage of muscle development. Previously, elevated activity of P2X7 receptors and increased store-operated calcium entry were shown in myoblasts derived from *mdx* mice. Here, the metabotropic extracellular ATP/UTP-evoked response has been investigated. Sensitivity to antagonist, effect of gene silencing and cellular localization studies showed that elevated purinergic responses in *mdx* myoblasts have been caused by increased expression of P2Y2 but not P2Y4 receptors. These alterations have physiological implications as shown by reduced motility of *mdx* myoblasts upon treatment with P2Y2 agonist. The ultimate increase in intracellular calcium in dystrophic cells reflected complex alterations of calcium homeostasis identified in the RNA seq data and with significant modulation at the protein level including a decrease of Gq11 subunit α, PMCA, IP3-receptor and elevation of PLCβ, SERCA and NCX. In conclusion, whereas specificity of dystrophic myoblast excitation by extracellular ATP is determined by specific receptor overexpression, the intensity of this altered response depends on relative activities of downstream calcium regulators that also accompany the *Dmd* gene mutation. These results confirm that phenotypic effects of DMD emerge in undifferentiated muscle cells and not only due to the absence of dystrophin protein in myofibres. Therefore, the pathogenesis of DMD and the relevance of current therapeutic approaches may need re-evaluation.

1. Introduction

Duchenne muscular dystrophy (DMD) is a lethal inherited disorder causing severe progressive muscle loss with sterile inflammation accompanied by cognitive and behavioural impairments and decreased bone strength. The disease is caused by the lack of dystrophin due to out-of-frame mutations in the DMD gene and the diversity of symptoms illustrates the importance of dystrophin in a range of cells. Indeed, DMD is the largest human gene known with 79 exons encoding 3 full-length (427 kDa) expressed in temporally-controlled and tissue-specific manners in muscle but also in non-muscle cells. The five progressively-

shortened isoforms (Dp412, Dp260, Dp140, Dp116 and Dp71) also present specific spatio-temporal patterns of expression, occurring as early as in embryonic stem cells and they have distinct roles, which are only partially understood [1]. Therefore, DMD is a multi-functional gene with a complex spatio-temporal expression pattern. Yet, since the life-threatening effects of DMD mutations present in striated muscles, investigations have focused on the full-size dystrophins, which have been attributed with the key role in protecting myofibres. Dystrophin there localizes to the cytoplasmic face of the sarcolemma where it anchors a set of dystrophin-associated proteins (DAP) tethering this complex to the intracellular cytoskeleton and extracellular matrix proteins [2]. The current understanding is that the dystrophin-DAP provides structural stability to the myofibre sarcolemma and its loss triggers muscle degeneration by destabilization of this membrane, allows extracellular Ca^{2+} influx leading to abnormal intracellular calcium signalling and a downstream cascade eventually resulting in muscle cell death. The evidence for this mechanical/structural instability triggering this complex train of pathological events is that the re-expression of dystrophin improves structure and function of dystrophic muscles. However, this does not necessarily prove that the disease starts with the absence of dystrophin in myofibres. Indeed, RNAi mediated knock-down of the full-length dystrophin expression in adult mouse did not trigger muscle degeneration despite a loss of protein from the sarcolemma [3]. Furthermore, the knockout of the DAP protein dystroglycan in mature muscle was associated with loss of dystrophin from the sarcolemma but caused no necrosis or sarcolemmal fragility [4]. These results indicate a need for critical re-evaluation of current views regarding the pathogenesis of DMD and the therapeutic strategies being developed [5]. It is important to consider whether the absence of dystrophin in fully differentiated muscle fibres is the mechanism of disease and therefore, whether dystrophin re-expression in myofibres would cure this disease. Indeed, dystrophin is expressed early in embryogenesis (mouse E9.5) and its absence in *mdx* mouse severely disrupts muscle development due to stem cell loss and disrupted muscle patterning [6]. The absence of DMD gene expression also affects stem cells leading to the intrinsic exhaustion of stem cells pool thus compromising muscle regeneration [7, 8]. This abnormality has been linked to the absence of the full-length dystrophin in activated satellite cells, where it regulates cell polarity and reduced number of myogenic progenitors [9]. A recent study linked the DAP in muscle stem cells undergoing asymmetric division with the epigenetic activation [10]. Furthermore, myogenic cells from both Duchenne patients [11, 12] and *mdx* mice [13] show abnormalities of a range of important functions including altered proliferation and differentiation and defects of energy metabolism with disorganized mitochondrial networks [14]. Moreover, a purinergic phenotype involving an increased expression and activity of P2XR7 receptors has been identified in myoblasts of the *mdx* mouse model of Duchenne type muscular dystrophy [15, 16] as well as in human DMD lymphoblasts [17]. Further analyses led to a discovery of a novel mechanism of P2XR7-evoked autophagic death in dystrophic muscle [18]. Finally, ablation or pharmacological inhibition of P2RX7 significantly reduced the disease progression in the mdx model of DMD [19, 20, 21].

Besides the aberrant ionotropic response to extracellular ATP, we have also found increased activity of store-operated calcium entry mechanisms in dystrophic myoblasts [22]. These and other studies demonstrate that abnormalities of calcium homeostasis in DMD occur in myoblasts and not only in fully differentiated myofibres and that they involve alterations of

specific cellular mechanisms rather than mechanical membrane instability.

Indeed, here we present evidence of a profound alteration of calcium homeostasis in myoblasts with the mutant *Dmd* gene, which involves the metabotropic response to eATP combined with dysregulation of the intracellular calcium machinery. Substantially increased activity of P2RY2 was identified in ATP- or UTP- stimulated dystrophic mouse myoblasts. While this effect could be attributed to the increased P2RY2 levels in the plasma membrane, the specificity of calcium responses in *mdx* myoblasts extends beyond the stimulation of P2RY2. The height and shape of elevated calcium transients reflect the combination of both the increased receptor activity and other significantly altered proteins involved in calcium signalling regulation in these cells.

2. Material and Methods

2.1 Cell culture

Immortalized mdx mouse and dystrophin-positive control (w/t) myoblasts were used. These two cell lines were of the same genetic background, as the two mouse strains from which the cells were derived originated from the same parental inbred mouse strain H2Kb-tsA58 ("immorto mouse"), expressing the SV40 large T antigen gene with the tsA58 mutation. The H2Kb-tsA58 mdx strain was established by crossing male mouse homozygous for H2Kb-tsA58 with female mdx mice [23]. *Mdx* and w/t cells used here are highly homogenous populations differing only in the presence or absence of a point mutation in the dystrophin gene exhibiting muscle phenotype and myogenic potential following differentiation [16, 24, 25, 26]. Cells were cultured in Dulbecco's modified Eagle's medium (DMEM, Sigma Chemical Company, St. Louis, MO, USA) supplemented with 20% fetal calf serum, 4 mM L-glutamine, 100 unit/ml penicillin, 100 μg/ml streptomycin, and 20 unit/ml murine γ-interferon (Invitrogen, San Diego, CA, USA) at 33°C. Under such conditions a differentiation of these cells was efficiently prevented. Moreover both cell lines were also cultured at 37°C in absence of γ-interferon in KnockOut DMEM (Invitrogen) supplemented with 10% v/v KSR (Knockout Serum Replacement, Invitrogen), 5% v/v DHS (Donor Horse Serum, Sera Labs) and 2 mM L-glutamine. Under these conditions the cells exhibits phenotypic properties of primary myoblasts. Such an approach allows to maintain primary-like ("de-immortalised") cells because of prevented expression of the rtsA58-mutated T-large antigen-encoding gene.

2.2 RNAseq

Immortalised myoblast cell lines were cultured in immorto conditions to produce 4 populations of each genotype growing apart for 2 passages and then replated and cultured for 48 hours in primary myoblast conditions at 37°C with 5 % CO_2 in IFN-γ free medium (see above).

Total RNA was extracted using an RNEasy plus universal mini kit (QIAGEN 73404) following manufacturer's instructions. Briefly, cells were washed 3 times with warm DPBS before being lysed directly on the culture plate by adding QIAZOL lysing buffer and using a cell scraper to disrupt the cells. Samples were then treated as per provided protocol.

After extraction, total RNA samples were sent to THERAGEN ETEX (Republic of Korea) for quality control and sequencing. Quality was assessed using an Agilent Bioanalyzer 2100, with a minimum RNA integrity number (RIN) of 7.0 or greater being required. Libraries were prepared using an Illumina TruSeq stranded total RNA kit, including ribodepletion using the Ribo-Zero Human/Mouse/Rat kit to remove ribosomal RNA. Libraries were sequenced in a paired-end 100bp run using an Illumina HiSeq 2500 sequencing platform.
Quality control of raw fast reads was conducted using fastQC [27]. Reads were trimmed using trim-galore [28] with parameters-to remove adapter sequence and low quality sequence tails. Trimmed reads were mapped against the GRCm38 *Mus musculus* genome from Ensembl using the STAR universal RNA seq aligner [29] with parameters '"--outSAMmultNmax 300 --outSAMstrandField intronMotif".

Differential expression analysis was conducted using the DESeq2 package [30] in R [31]. Gene models were taken from Ensembl version 91, and read counts over unique genes were quantified using the summarize Overlaps function in the GenomicAlignments package [32] using mode "Union". P values were adjusted for multiple testing by using the Benjamini and Hochberg correction [33]. Significantly differentially expressed genes were identified based on a fold-change of 2-fold or greater (up- or downregulated) and an adjusted p-value less than 0.05. Gene ontology analysis was conducted using the clusterProfiler package [34].

2.3 RNA extraction, reverse transcription and quantitative RT-PCR

Total RNA was isolated using Trizol method (TRI reagent, T9424; Sigma). The quality and quantity of samples were determined using a NanoDrop spectrophotometer. Only RNA with an absorbance ratio 260/280 between 1.8 - 2.0 was used to reverse transcription. Complementary DNA (cDNA) was synthesized from 2 µg of total RNA using First Strand cDNA Synthesis Kit with M-MLV reverse transcriptase and oligo(dT) primers (#K1612, Thermo Fischer Scientific), according to the manufacturer's instructions.

RT-qPCR was performed using TaqMan Fast Universal PCR Master Mix (4352042, Applied Biosystems) and TaqMan Gene Expression Assays (the primers ID: Mm 01274119_m1 for P2RY2, Mm 00445136_s1 for P2RY4) on the 7500 ABI Prism Real-Time PCR System (Applied Biosystems). The level of expression of target genes were normalized to the expression of GAPDH (primer ID: Mm99999915_g1) housekeeping gene. Analysis of relative gene expression data were determined by 2-ΔΔCt method using StepOne Software.

2.4 Cell lysis, protein extraction and analysis

Proteins were extracted from adherent cells by scraping into extraction buffer (1x LysisM, 1x protease inhibitor cocktail, 2 x phosphatase inhibitor cocktail (all Roche), 2 mM sodium orthovanadate (Sigma) suspending with the use of automatic pipets followed by repeatedly forcing through the syringe needle (0.5 mm in diameter) and incubation of the suspension on ice for 20 min. After centrifugation (15 000 x g, for 20 min at 4^{o}C) protein concentrations in supernatants collected were determined using a Bradford protein assay (Bio-Rad). Remaining supernatants were mixed with sample buffer at 3:1 $^{v}/_{v}$ ratio, heated for 5 min at 95°C and chilled on ice and stored at -20^{o}C. Proteins (20 µg of each sample) were separated on 0.1% SDS-polyacrylamide gels (6-12% $^{w}/_{v}$ depending on the molecular mass of protein) and electroblotted onto Immobilon-PVDF Transfer Membrane (Merck Millipore). Blots were

blocked in 5% $^{w}/_{v}$ non-fat milk or 5% BSA (Albumin, Bovine Serum, 12659, Merck Millipore) powder solved in 1 x TBST, 0.01% $^{v}/_{v}$ Tween-20 (Sigma) for 1h at room temperature (RT) prior to probing with appropriate primary antibody diluted in a blocking buffer containing 2.5% milk or 5% BSA (incubated overnight at 4ºC with agitation). To identify proteins of interest following primary antibodies were applied: P2RY2 (1:270, APR-10) and P2RY4 (1:300, APR-006; all Alomone Labs), calsequestrin (ab126241), calreticulin (ab128885), SERCA1 (ab124501) and SERCA2 (ab91032; all diluted 1:1000, Abcam), Gαq11 (1:1000, 06-709 Merck Millipore), PLCβ isoforms 1-4 (sc-5291, sc-515912, sc-133231, sc-166131, respectively; all diluted 1:100, Santa Cruz Biotechnology), NCX1 (1:1000, R3F1 Swant) and NCX3 (1:500, ab84708 Abcam) and IP3R (diluted 1:1000 in BSA solution as described above, #8568 Cell Signaling Technology). Then membranes were washed (3x) with 1x PBST for 10 min each wash and incubated with anti-Rabbit (diluted 1:5000, ab6721, Abcam) or anti-Mouse (1:3000, ab6728, Abcam) horseradish peroxidase-conjugated secondary antibody for 1h at RT.

Specific protein bands were visualized using luminol-based substrates (Millipore) and images obtained using a Fusion FX (Vilber Lourmat). β-tubulin (1:10000, ab21058), Na+-K+ ATPase (1:200, ab7671) and caveolin (1:2000, ab2910; all Abcam) antibodies were used as a protein-loading control dependent on the protocol. Densitometric analyses of specific protein bands were made using exposure times within the linear range and the integrated density measurement function of BIO-1D (Vilber Lourmat). All experiments were repeated at least 3 times with similar results obtained in each replicate.

2.5 siRNA transfection

P2RY2 gene silencing was performed with the use of short interfering RNA (Silencer Select Pre-designed siRNA ID #s71197, Invitrogen, Thermo Fisher Scientific. Scrambled siRNA oligonucleotide (Silence Select Negative Control Scramble siRANA #4390847, Invitrogen) was used as a negative control. The sequence of P2RY2 siRNA were as follows:
sense sequence 5'- CCGUAAUCCUGGUCUGUUAtt -3'antisense sequence 3'-UAACAGACCAGGAUUACGGaa -5'.
Mdx and wt myoblasts were transfected with 50 nM siRNA using 3 µl/ml Lipofectamine RNAiMAX (#13778, Invitrogen). The transfection was carried out for 72 h in the medium as described above but without antibiotics and then cells were collected and analysed by Western blotting.

2.6 Isolation of the plasma membrane fraction

For isolation of membrane, around 25 x 106 cells were trypsinised, washed in ice-cold PBS, collected by centrifugation at 200 x g for 3 min and the cell pellet washed again with ice-cold PBS and finally the pellet was resuspend in cold Buffer A included in commercial Plasma Membrane Protein Extraction Kit (101Bio, #P503, Thermo Fisher Scientific). The isolation of the plasma membrane proteins was carried out according to the manufacturer's instruction. The extract plasma membrane proteins were analysed by Western blotting as described above.

2.7 $[Ca^{2+}]_c$ measurements in myoblasts in vitro

Myoblasts were cultured on glass coverslips in a 6-well plate (500 000 cells/well) for 48 h under conditions described above. Cells (70–80% confluent) were loaded with 1 μM Fura 2 AM (Molecular Probes, Oregon) in culture medium for 15 min at 33°C in a humidified atmosphere of 95% O_2 and 5% CO_2. The cells were then washed twice with the solution composed of 5 mM KCl, 1 mM $MgCl_2$, 0.5 mM Na_2HPO_4, 25 mM HEPES, 130 mM NaCl, 1 mM pyruvate, 5 mM D-glucose, and 0.1 mM $CaCl_2$, pH 7.4 and the coverslips were mounted in a cuvette containing 3 ml of either the nominally Ca^{2+}-free assay solution (as above but 0.1 mM $CaCl_2$ was replaced by 0.05 mM EGTA) or Ca^{2+}-containing assay solution (as above but with 2 mM $CaCl_2$) and maintained at RT in a spectrofluorimeter (Shimadzu, RF5001PC).

Fluorescence was recorded at 510 nm with excitation at 340 and 380 nm. At the end of each experiment the Fura 2 fluorescence was calibrated by addition of 8 μM ionomycin to determine maximal fluorescence followed by addition of EGTA to complete removal of Ca^{2+}. Cytosolic Ca^{2+} concentration $[Ca^{2+}]_c$ was calculated according to Grynkiewicz et al. [35]. The cells were treated with 500 μM and 1 mM ATP, 100 μM and 500 μM UTP (both Sigma) and 10 μM AR-C 118925XX (216657-60-2, TOCRIS Bioscience) applied 10 min prior to the addition of ATP and UTP. Each experiment was repeated at least 5 times.

2.8 Immunocytofluorescence (ICC)

Cells were cultured on coverslips (50-60 %) in growth medium. After rinsed twice with cold PBS (w/o calcium and magnesium) the myoblasts were fixed in a 4% $^{w}/_{v}$ paraformaldehyde solution (PFA) in PBS for 15 min on ice. Then cells were permeabilized using PBS with 0.1% Triton X-100 for 5 min and blocked in a 5% $^{v}/_{v}$ goat serum (GS, Normal Goat Serum, S-1000, Vector Laboratories IVD) in PBS for 1 h at RT and incubated overnight at 4°C with primary antibodies (anti-P2RY2 and anti-P2RY4, as described above, diluted 1:100 in blocking buffer). The secondary antibody (diluted 1:1000 in 5% GS in PBS, Alexa Fluor®488 goat anti-Rabbit, Thermo Fisher Scientific) was added for 1 h RT in dark. Then myoblasts were rinsed 3 times for 10 min each wash with agitation between each steps of ICC protocol. After staining, cells on coverslips were mounted onto microscope slides sealed in Glycergel Mounting Medium with DAPI (H-1200 VectaShield®, Vector Laboratories) prior to imaging. Images were obtained using a confocal microscope (Zeiss Spinning Disk Confocal Microscope) and image analysis was performed by using ImageJ software.

2.9 Random motility assay

To perform random migration assays 15,000 myoblasts (*mdx* and w/t) were seeded into 24-well cell culture plate and grown for 30 h in an appropriate culture medium. Then, multiple different well areas per each cell type were photographed in the bright field or DIC Nomarski contrast using HC PL APO 10x/0.40 Dry objective (Leica Microsystems GmbH) every 15 min for 6 h on inverted DMI6000 microscope (Leica Microsystems GmbH) equipped with DFC350FXR2 CCD camera (Leica Microsystems GmbH) and an environmental chamber (PeCon GmbH). Acquired time-lapse movies were exported to TIFF format and aligned to compensate possible drift using an ImageJ plugin. Subsequently, at least 15 cells of each experimental condition were tracked semi-automatically in the time-lapse movies using Track Objects plug-in in Leica MM AF powered by MetaMorph® software

(Leica Microsystems GmbH). Cells dividing or colliding with other cells were excluded from the analysis. Obtained cell coordinates were subsequently imported into Matlab R2016b software (MathWorks, Inc.) and the movement parameters were calculated using a Matlab script. Each experiment was performed at least in triplicate. Statistical analysis was performed using Student's *t* test.

2.10 Data analysis

Data are expressed as a mean value ± standard deviation (SD). Statistical significance was assessed by Student's t-test A p value of <0.05 was considered statistically significant where n=3-5 for PCR and Western data, and n=3-9 for other analyses ("n" represents the number of independent experiments with cells derived from different passages).

3. Results

3.1 ATP sensitive nucleotide receptors

RNASeq analysis was performed as described to identify key transcription alterations between dystrophic (referred to as *mdx*) and wild type (w/t) myogenic immorto cells cultured under the primary myoblast conditions (Young et al., 2015, 2018). Differential expression analysis revealed a striking global transcriptional change as a result of the mdx mutation, with 996 genes upregulated and 1,134 genes downregulated in dystrophic myoblasts (Fig. 1A and B). While global differential expression analyses will be presented elsewhere (manuscript in preparation), here we focussed on the purinergic phenotype, which is clearly caused by the *Dmd* gene mutation. In particular, we confirmed significant upregulation (4.8-fold increase, p = 7.39e-40) of the P2RX7 transcript, which has been previously categorised (Yeung et al., 2006, Young et al., 2012, etc.). In addition, we saw significant differential expression, albeit at lower magnitude, for P2RX4 (1.8-fold increase, p = 1.16e-16) and P2RX6 (1.5-fold downregulated, p = 7.02e-6). Conversely, no significant differences were seen for P2RX5 (Fig. 2).

Stimulation with ATP or UTP in the presence of 2 mM $CaCl_2$ in the extracellular milieu resulted in a transient increase in the cytosolic [Ca^{2+}], that was substantially stronger in *mdx* than w/t cells (Suppl. Fig 1). Under such experimental conditions, $[Ca^{2+}]_c$ peak is a resultant of at least three mechanisms directly responsible for the elevation of cytosolic Ca^{2+} concentration. These include: (i) Ca^{2+} influx through P2RX channels and (ii) store-operated calcium entry (SOCE), which both allow extracellular Ca^{2+} to flow into the cell. Both mechanisms have been identified and analysed by us previously in immortalized and primary w/t and *mdx* myoblasts [15, 22]. The third mechanism concerning the eATP-evoked response is Ca^{2+} release from the ER stores due to stimulation of metabotropic nucleotide receptors of the P2RY family. This step is also a prerequisite for SOCE. Moreover, the height and temporal pattern of the [Ca^{2+}]c peaks, irrespectively of their origin, are modified by other processes shaping calcium transients in excited cells.

To avoid a concomitant stimulation of P2RXs (by ATP) or an activation of the store-operated Ca^{2+} entry following depletion of the ER stores, calcium responses of myoblasts to ATP or UTP were tested under Ca^{2+}-free conditions. Thus, an intensity of calcium release from the ER was first of all considered as a resultant of activities of P2RYs and other proteins involved in the PM–ER signal transduction.

Fig. 3 displays a calcium response of w/t and *mdx* myoblasts to ATP (Fig. 3A and B) or UTP (Fig. 3C and D). These agonists stimulate both P2RY2 and P2RY4 but ATP additionally exhibits small affinity to other P2RYs while UTP is particularly specific to P2RY2. Wild type myoblasts were only slightly susceptible to stimulation by ATP or UTP while *mdx* strongly responded to both nucleotides.

Significant differential expression was detected in the RNA seq data for P2RY receptors P2RY1 (13.6-fold upregulated, p = 5.69e-3), P2RY2 (5.9-fold upregulated, p = 4.84e-4), and P2RY6 (4.8-fold downregulated, p = 2.09e-2), although detection of these genes was very low (FPKM < 0.2). P2RY4 was almost undetectable and showed no change in *mdx* samples. Given the increased metabotropic response to eATP in dystrophic cells, and our previous studies, which indicated a P2RY component in the purinergic response in *mdx* cells [15], we performed qPCR and Western blotting analysis of P2RY2 and P2RY4 (the two P2Y receptors responding to eATP) to validate the results from the RNA seq with more sensitive assays. As with the RNAseq data, much higher levels of P2RY2 transcript were found by qPCR in *mdx* compared to w/t myoblasts (Fig. 4), whilst P2RY4 was undetectable by qPCR. Surprisingly however, a band corresponding with the predicted molecular mass of P2RY4 receptor was detected by Western blotting and this band was substantially stronger in *mdx* than in w/t myoblasts (Fig. 4). However, further analysis of plasma membrane proteins revealed that the P2RY2 was predominantly found in the membrane fraction and with significantly increased levels in dystrophic myoblasts (Fig. 5 and 6). In contrast, P2RY4 band was present in the cytosol but almost undetectable in the membrane fraction of *mdx* and w/t cells. This cellular localisation made the putative receptor contribution to the extracellular ATP responses rather unlikely. Immuno-localisation of P2RY2 receptor in myoblasts membrane (Fig. 6) confirmed this conclusion but also revealed a strong signal in the nuclei in addition to cytoplasmic staining.

Indeed, substantially reduced calcium response to ATP or UTP in the presence of a specific P2RY2 antagonists (AR-C118925XX) (see. Fig. 3) confirmed a leading role of P2RY2 in this process. UTP-evoked calcium response is selective and therefore more efficiently blocked by AR-C118925XX. Finally, inhibition of UTP-induced Ca^{2+} release in cells with siRNA silenced P2RY2 expression confirmed calcium response to be P2Y2-evoked (Fig. 7). This approach also allowed us to confirm the specificity of the band detected with anti-P2RY2 antibodies. This was important as the in-gel mobility of this protein reported by various authors differs significantly [36. 37, 38 39]. As shown in Fig. 7, the band of a reduced intensity upon treatment of cells with P2RY2-specific siRNA corresponds to protein of a molecular mass slightly below 70 kDa, which is in agreement with data previously published by Choi et al., 2013 [36]. In summary, the qPCR transcript expression data in agreement with increased P2RY2 protein, silencing and pharmacological inhibitor study were all in line with the P2RY2 being responsible for the elevated nucleotide-evoked Ca^{2+} release in dystrophic myoblasts (Fig. 3). Importantly, we further found that the elevated P2RY2 and an increased intensity of calcium response upon stimulation of dystrophic myoblasts with UTP causes a functional cellular response. As shown in Fig. 8, unstimulated *mdx* myoblasts are substantially more mobile than w/t cells and their motility was reduced in the presence of UTP. Although also observed in w/t cells, this effect has not been significant (Fig. 8). Some

degree of inhibition of this UTP action by AR-C118925XX additionally confirmed the role of P2RY2 receptor. Similar effect of UTP was previously described in leukaemic cells [40].

2.2 Calcium signalling toolkit

In view of a high complexity of a regulation of intracellular calcium signalling, the increased $[Ca^{2+}]c$ upon stimulation of *mdx* myoblasts with ATP or UTP probably cannot be explained exclusively by the elevated P2RY2 level in the plasma membrane. Therefore, to gain insight into this mechanism, we have analysed the RNA seq data for possible changes in expression of genes involved in calcium homoeostasis. Gene ontology analysis of genes showing differential expression in the dystrophic cells showed significant enrichment for genes involved in regulation of calcium ion transport into cytosol ($p = 1.54e^{-3}$), whilst global analysis of 870 genes involved in calcium ion transport, binding, and homeostasis functions identified significant modulation (both up and down-regulation) in dystrophic cells (Fig. 9).

To investigate this newly identified abnormality in calcium signalling, we have estimated a relative amount of Ca^{2+} stored in dystrophic and control myoblasts. Moreover, levels of calcium signal transducing proteins linking P2RY2 receptor with the ER calcium stores have been compared. Fig. 10 A shows that a treatment of cells with ionomycin under Ca^{2+}-free conditions resulted in a fast and transient increase of cytosolic Ca^{2+} concentration due to Ca^{2+} release from intercellular stores. Since mitochondrial uncoupling with FCCP does not influence Ca^{2+} concentration in cytosol (data not shown) it may be assumed that the entire cytosolic Ca^{2+} originates from the ER. Ionomycin distributes evenly among cellular membranes thus an elevation of cytosolic Ca^{2+} concentration is due to a fact that the Ca^{2+} concentration between ER and cytosol equilibrates much faster than that between cytosol and extracellular milieu. It probably mirrors the proportion between surface area of the ER and PM membranes [41]. Though such a ploy does not allow calculating Ca^{2+} content in the ER in the absolute units, it may be useful to compare a total amount of Ca^{2+} stored in various cells or under different conditions. Thus, a greater increase of cytosolic Ca^{2+} concentration in *mdx* myoblasts than in the w/t cells upon treatment with ionomycin indicates that the former accumulate more Ca^{2+} in the ER. Additionally, *mdx* myoblast contain more calsequestrin (Fig. 10 B) while the calreticulin level is unaltered by the *mdx* mutation (Fig. 10 C). This finding may suggest higher calcium storage capacity of *mdx* myoblasts and is in line with greater amount of Ca^{2+} released upon treatment of these cells with ionomycin (Fig. 10 A). In addition, substantially elevated level of SERCA1 and SERCA2B proteins (Fig. 11), which are to reload ER stores with Ca^{2+}, fits well with the concept of increased abundancy of cellular calcium stores in *mdx* myoblasts.

Altogether, these results may suggest that the increased calcium release in dystrophic cells results not only from the higher level of P2RY2 protein in the plasma membrane but also from the increased amount of Ca^{2+} stored. This could give a misguided impression of an elevated P2RY2 activity or at least result in overestimation of its contribution to the intensity of calcium responses. Stimulation of P2RY2 activates signal transduction cascade, which may contribute to a regulation of the intensity of calcium response to metabotropic receptors stimuli. All results shown hitherto are clearly in line with an elevation of calcium release from the ER upon treatment of cells with ATP or UTP. Therefore, decreased level of Gq_{11} protein shown in Fig. 12 A have been unexpected. This protein mediates P2RY-dependent activation

of Ca^{2+} release from the ER, thus the decreased amount of it is inconsistent with a logical assumption suggesting an enhanced signal transduction from P2RY2 to the ER. In contrast, Gi and Gs protein levels were unchanged in *mdx* myoblasts (data not shown).

In a view of the slightly elevated calcium content in the ER, it is tempting to speculate that lowered Gq/11 subunit α protein content may be an element of a cellular defence mechanism that protects myoblasts from an excessive Ca^{2+} release and increased cytosolic Ca^{2+} concentration upon activation of P2YR2. This suggestion also concerns the substantially reduced level of IP3 receptor (Fig. 12 B), which is responsible for Ca^{2+} release upon binding IP3 produced from phosphatidylphosphoinositol, which hydrolysis is catalysed by PLC). On the other hand, a considerably increased level of PLCβ isoform 4 (Fig. 13 D), which is responsible for increasing IP3 concentration, is in line with increased Ca^{2+} release and could counterbalance reduced protein G and IP3R content. To summarize, the significantly stronger calcium response of *mdx* myoblasts treated with ATP or UTP is probably a result of a few counteracting changes in specific proteins identified in this study.

It must be stressed however, that Fura-2 allows measuring of cytosolic Ca^{2+} concentration, which depends on two classes of events: Ca^{2+} entry into cytosol (from the ER and extracellular space) and opposite processes responsible from Ca^{2+} removal from cells and its uptake and storage by the ER. As shown in Fig. 14 cellular level of PMCA protein is substantially lower in *mdx* myoblasts than in the w/t cells. This Ca^{2+}-pump exhibits high affinity to calcium cation but it works relatively slowly, thus is thought to be responsible for maintaining low Ca^{2+} concentration in resting cells. On the other hand, an elevated level of sodium-calcium exchangers (NCX1 and 3) suggests an increased efficiency of calcium removal during a recovery phase following cell excitation. This mechanism allows cells to restore resting Ca^{2+} concentration and presumably shapes $[Ca^{2+}]c$ transients. Data shown in Fig. 14 suggest that Ca^{2+} transients due to calcium release from the ER, which are much higher in the *mdx* myoblasts than in their control equivalents, may be attenuated by counteracting processes of Ca^{2+} removal from the cytosol.

Furthermore, to establish the compatibility with the data we previously obtained in *mdx* and *w/t* cells grown under "immorto" conditions we have repeated selected experiments and confirmed the results in such cells (Fig Suppl. 1-6).

4. Discussion:

Precise regulation of nucleotide-induced calcium signals is of high importance in stimulated and differentiating satellite cells. This may be accomplished due to a concerted activities of numerous "molecular tools" engaged in Ca^{2+} transport, sensing and storage, which are involved in a spatio-temporal controlling of changes in local and global cytosolic $[Ca^{2+}]$. Moreover, an excitation of cells via metabotropic receptors needs a contribution of several factors, which form a signal-transforming cascades. Purinergic P2Y receptors belong to this category. Available data indicate that the pattern of their expression changes during muscle maturation from satellite cells through myoblasts to fully differentiated muscle fibres [42]. As a proliferation and differentiation of dystrophic myoblast seems to be accelerated in comparison to the w/t cells [13] it is probable that their nucleotide-evoked calcium response may differ [43, 44]. Previously we showed an increased susceptibility of *mdx* myoblasts to

P2XR7-mediated stimulation by ATP. It resulted in an accelerated calcium entry into *mdx* cells and was correlated with an elevated expression of P2XR7 protein [16]. Moreover, prolonged stimulation of *mdx* myoblasts with ATP or more selectively with P2RX7-specific agonist BzATP led to the opening of a large pore and additional effects such as stimulated autophagy and MMP-2 release [18, 45]. In these cells as well as in the primary *mdx* myoblasts an increased level of STIM1 protein seems to be behind significantly increased store-operated calcium entry (SOCE) [22]. In this paper the first step of cellular response to a stimulation of metabotropic nucleotide receptors, leading to a depletion of ER stores which is prerequisite for SOCE activation has been investigated. This is also the "metabotropic" complement to the previously characterized ionotropic response of *mdx* myoblasts to ATP [15].

All findings here together with those published previously [15, 22] clearly indicate that calcium signalling in *mdx* myoblasts and w/t cells varies and the amplitude of calcium response is always higher in the *mdx* myoblasts than in their w/t equivalents. In this study mice myoblasts were stimulated with ATP or UTP under calcium-free conditions to avoid any P2X-dependent calcium entry (in a case of ATP as a stimulus) and an activation of the store-operated calcium entry. Both agonists may activate P2RY2 and P2RY4. In fact, ATP may slightly activate some other P2RYs, however considering a particularly high selectivity of this nucleotide to P2RY2 and P2RY4, we focussed on P2RY2 and P2RY4 in further studies. Slightly lower response of cells to 1 mM than to 0.5 mM ATP may be due to additional effects coming from a stimulation of other ATP-sensitive proteins putatively leading to an reciprocal inactivation of proteins on the outer surface of the plasma membrane [45]. Discriminating between P2RY2 and P2RY4 activities is difficult because of the lack of satisfactorily specific spectrum of pharmacological tools including agonists and antagonists selective for each of the two types of P2RYs tested. However, lack of detectable P2RY4 transcript expression in RNASeq and qPCR, a sensitivity to P2RY2-specific antagonist and inhibitory effect of silencing of P2RY2 expression indicate that P2RY2 is a predominant receptor activated in *mdx* myoblast treated with ATP under Ca^{2+}-free conditions. Under these circumstances, finding of an anti-P2RY4 reactive band in the total homogenate of *mdx* myoblasts was confusing. However, absence of P2RY4 protein in the plasma membrane of all tested cells excludes its contribution to the observed purinergic calcium response. P2RY4 localised inside cells, presumably in an inactive form (e.g in secretory granules) but not in the plasma membrane might correspond to a freshly synthesised protein and point to "a higher readiness" of *mdx* cells to a response via a P2YR4-dependent mechanism to potential stimuli. Similar cytosolic localisation of P2RY4 was previously found in HT-29 human colon cancer cells [46]. Suppl. Figs. 4 and 5 also indicate lack of P2RY4 protein in the plasma membrane of immortalised w/t and *mdx* myoblasts.

The nuclear staining with P2RY2 antibody probably reflects its poor specificity. In fact Western blot of proteins from isolated nuclei probed with P2RY2 antibodies showed a band corresponding to much smaller protein (data not shown) which intensity was insensitive to P2RY2 gene silencing.

A functional identification of the P2RY2 as a receptor responsible for ATP/UTP-induced metabotropic calcium response of *mdx* myoblasts together with elevated plasma membrane protein levels suggest a simple cause-effect explanation of increased susceptibility of dystrophic cells to this nucleotide. However, we uncovered a further significant modulation

of cellular calcium homeostasis in dystrophic myoblasts.

RNASeq and biochemical data shown here indicate a set of changes which may affect calcium signalling in *mdx* myoblasts. They include changes in signal-transducing processes down-stream to the plasma membrane receptors. Subtle interplay between "on and off" mechanisms leads to a balanced elevation of calcium responses, which fulfil the cellular demand. Final intensity of the calcium signal is a resultant of many, sometimes opposite, regulatory processes. Such a complex regulation prevents cell overloading with calcium. Increased amount of P2RY2 and PLC proteins as well as the increased abundance of the ER calcium stores may explain the increased Ca^{2+} release from the ER. On the other hand, substantially reduced level of Gq11 subunit α and IP3R counteract the elevated signal transduction. It seems possible that the type of receptor decides the specificity of cellular response while its intensity might be further regulated by a very broad toolkit composed of proteins involved in calcium signalling. Special attention should also be paid to proteins involved in the restoration of the resting cytosolic Ca^{2+} concentration: NCX, SERCA and PMCA as they are directly involved in regulating/shaping calcium signals regardless of a mechanism behind the induction of cellular calcium response.

Thus, results shown here complement the general picture describing differences in the pattern of molecular tools (channels, pumps, exchangers, buffers) responsible for Ca^{2+} homeostasis in w/t and *mdx* myoblasts. A scheme shown in Fig. 15 summarizes data shown here and in two previous papers [15, 22]. We propose that *mdx* mutation affects proportions between particular processes engaged in the intracellular calcium signalling.

Results presented in this paper are in line with the hypothesis that phenotypic effects of *mdx* mutation occur as early as in undifferentiated muscle cells. Expression of full-length dystrophin transcripts in muscles is developmentally regulated: The satellite cells and proliferating myoblasts do not have detectable levels of dystrophin protein, while it is found in myotubes/myofibres. This observation, understandably, led to the commonly postulated hypothesis that dystrophin mutations would have an impact in differentiated muscles only and, as a result, research into the mutant phenotype has focused on the absence of dystrophin in myofibres sarcolemma. Thus phenotypic effects of the DMD mutations have usually been analysed in differentiated muscle cells as being unexpected at earlier stages of muscle development. In contrast to this well-established belief, many well documented experimental data indicate multiple phenotypic changes in undifferentiated cells with mutant dystrophin gene. Although the molecular mechanism behind such a broad spectrum of changes of $[Ca^{2+}]c$ regulatory mechanisms caused by *mdx* mutation in mice myoblasts is still elusive, data shown here strengthen a hypothesis of a very early (in terms of muscle cell differentiation) onset of Duchenne type muscular dystrophy. It sheds new light on DMD pathophysiology and might be potentially important for pharmacological alleviation of DMD symptoms [5].

We also demonstrated that these changes are due to *Dmd* gene mutation and not caused by cell immortalisation or being evoked by the effects of the dystrophic niche on primary myoblasts because these abnormalities are present in immortalized and de-immortalized cells alike. However, the results shown here should be verified in primary *mdx* cells similarly to what was done in previous studies [22], which make the observations shown here more reliable.

5. Conclusion

Mdx myoblasts exhibit an elevated P2RY2 stimulation. Receptor overexpression determines the selectivity of cell response while the intensity of calcium signal seems dependent on the modulation of a set of proteins responsible for intracellular signal transduction, Ca^{2+} transport and storage. Thus, the resultant Ca^{2+} response reflects activity of processes increasing $[Ca^{2+}]_c$ counterbalanced by mechanism, which prevent calcium overload. Diverse responses of w/t and *mdx* myoblasts to ATP or UTP and significant differences in RNASeq profiles confirm the hypothesis that phenotypic effects of DMD mutation occur as early as in undifferentiated muscle cells.

6. References

1. Doorenweerd N., Mahfouz A., van Putten M., Kaliyaperumal R., T'Hoen P.A.C., Hendriksen J.G.M., Aartsma-Rus AM., Verschuuren J.J.G.M., Niks E.H., Reinders M.J.T., Kan H.E., Lelieveldt B.P.F., 2017. Timing and localization of human dystrophin isoform expression provide insights into the cognitive phenotype of Duchenne muscular dystrophy, Sci. Rep. 7; 12575 Published online 2017 Oct 3. doi: 10.1038/s41598-017-12981-5PMCID: PMC5626779PMID: 28974727

2. J. Ehmsen, E. Poon, K. Davies, The dystrophin-associated protein complex, J. Cell Sci. 115 (2002) 2801–2803.

3. S.M.M Ghahraman, I.R. Graham, T. Athanasopoulos, C. Trollet, M. Pohlschmidt, M.R. Crompton, G. Dickson, RNAi-mediated knockdown of dystrophin expression in adult mice does not lead to overt muscular dystrophy pathology, Hum. Mol. Genet. 17 (2008) 2622-2632.

4. E.P. Rader, R. Turk, T. Willer, D. Beltrán, K-i. Inamori, T.A. Peterson, J. Engle, S. Prouty, K. Matsumura, F. Saito, M.E. Anderson, K.P. Campbell, Role of dystroglycan in limiting contraction-induced injury to the sarcomeric cytoskeleton of mature skeletal muscle, Proc. Natl. Acad. Sci. USA 113 (2016) 10992-10997.

5. Górecki D.C., 2016. Dystrophin: The dead calm of a dogma. Rare Dis. 4, e1153777. doi: 10.1080/21675511.2016.1153777

6. D. Merrick, L.K. Stadler, D. Larner, J.Smith, (Muscular dystrophy begins early in embryonic development deriving from stem cell loss and disrupted skeletal muscle formation, Dis. Model. Mech. 2 (2009) 374–388.

7. A. Sacco, F. Mourkioti, R. Tran, J. Choi, M. Lewellyn, P. Kraft, M. Shkreli, S. Delp, J.H. Pomerantz, S.E. Artandi, H.M. Blau, Short telomeres and stem cell exhaustion model Duchenne muscular dystrophy in mdx/mTR mice, Cell 143 (2010) 1059-1071.

8. F. Mourkioti, J. Kustan, P. Kraft, J.W. Day, M.M. Zhao, M. Kost-Alimova, A. Protopopov, R.A. DePinho, D. Bernstein, A.K. Meeker, H.M. Blau, Role of telomere dysfunction in cardiac failure in Duchenne muscular dystrophy, Nat. Cell Biol. 15 (2013) 895-904.

9. N.A. Dumont, Y.X. Wang, J. von Maltzahn, A. Pasut, C.F. Bentzinger, C.E. Brun, M.A. Rudnicki, Dystrophin expression in muscle stem cells regulates their polarity and asymmetric division, Nat. Med. 21 (2015) 1455-1463.

10. N.C. Chang, M-C. Sincennes, F.P. Chevalier, C.E. Brun, M. Lacaria, J. Segalés, P. Muñoz-Cánoves, H. Ming, M.A. Rudnicki, The Dystrophin Glycoprotein Complex Regulates the Epigenetic Activation of Muscle Stem Cell Commitment, Cell Stem Cells 22 (2018) 755-768. DOI:https://doi.org/10.1016/j.stem.2018.03.022.

11. G. Jasmin, C. Tautu, M. Vanasse, P. Brochu, R. Simoneau, Impaired muscle differentiation in explant cultures of Duchenne muscular dystrophy, Lab. Invest. 50 (1984) 197- 207.

12. B. Lucas-Heron, J.M. Mussini, B. Ollivier, Is there a maturation defect related to calcium in muscle mitochondria from dystrophic mice and Duchenne and Becker muscular dystrophy patients, J. Neurol. Sci. 90 (1989) 299-306.

13. Z. Yablonka-Reuveni, J.E. Anderson, Satellite cells from dystrophic (mdx) mice display accelerated differentiation in primary cultures and in isolated myofibers, Dev. Dyn. 235 (2006) 203-212. DOI: http://dx.doi. org/10.1002/dvdy.20602.

14. M. Onopiuk, W, Brutkowski, K. Wierzbicka, S. Wojciechowska, J,.Szczepanowska, J. Fronk, H.,Lochmüller, D.C. Górecki, K. Zabłocki, Mutation in dystrophin-encoding gene affects energy metabolism in mouse myoblasts. Biochem. Biophys. Res. Commun. 386 (2009) 463-466.

15. D. Yeung, K. Zabłocki, C-F. Lien, T. Jiang, S. Arkle, W. Brutkowski, J. Brown, H. Lochmuller, J. Simon, E.A. Barnard, D.C. Górecki, Increased susceptibility to ATP via alteration of P2X receptor function in dystrophic mdx mouse muscle cells, FASEB J. 20 (2006) 610-620.

16. C. Young, W. Brutkowski, C-F. Lien, S. Arkle, H. Lochmüller, K. Zabłocki, D.C. Górecki, P2X7 purinoceptor alterations in dystrophic mdx mouse muscles: Relationship to pathology and potential target for treatment. J. Cell. Mol. Med. 16 (2012) 1026-1037.

17. D. Ferrari, M. Munerati, L. Melchiorri, Hanau, S. F. Di Virgilio, O.R. Baricordi, Responses to extracellular ATP of lyphoblastoid cell lines from Duchenne muscular dystrophy patients, Am. J. Physiol. 267 (1994) C886-C892.

18. C.N. Young, A. Sinadinos, A. Lefebvre, P. Chan, S. Arkle, D. Vaudry, D.C. Gorecki,. A novel mechanism of autophagic cell death in dystrophic muscle regulated by P2RX7 receptor large-pore formation and HSP90. Autophagy 11(2015) 113–130.

19. Sinadinos A., Young C.N., Al-Khalidi R., Teti A., Kalinski P., Mohamad S., Floriot L., Henry T., Tozzi G., Jiang T., Wurtz O., Lefebvre A., Shugay M., Tong J., Vaudry D., Arkle S., doRego J.C., Górecki D.C., 2015. sP2RX7 purinoceptor: a therapeutic target for ameliorating the symptoms of duchenne muscular dystrophy, PLoS Med 12(10):e1001888

20. E. Gazzerro, S. Baldassari, S. Assereto, F. Fruscione, A. Pistorio, C. Panicucci, S. Volpi, L. Perruzza, C. Fiorillo, C. Minetti, E. Traggiai, F. Grassi, C. Bruno, Enhancement of muscle T regulatory cells and improvement of muscular dystrophic process in mdx mice by blockade of extracellular ATP/P2X Axis, Am. J. Pathol. 185 (2015) 3349–3360.

21. Al-Khalidi R., Panicucci C., Cox P., Chira N., Róg J., Young C.N.J., McGeehan R.E., Ambati K., Ambati J., Zabłocki K., Gazzerro E., Arkle S., Bruno C., Górecki D.C., 2018. Zidovudine ameliorates pathology in themouse model of Duchenne muscular dystrophy via P2RX7 purinoceptor antagonism. Acta Neuropath. Commun. (2018) 6:27. https://doi.org/10.1186/s40478-018-0530-4

22. M. Onopiuk, W. Brutkowski, C. Young, E. Krasowska, J. Róg, M. Ritso, S. Wojciechowska, S. Arkle, K. Zabłocki, D.C. Górecki, Store-operated calcium entry contributes to abnormal Ca^{2+} signaling in dystrophic mdx mouse myoblasts. Arch. Biochem. Biophys. 569 (2015) 1-9.

23. J.E. Morgan, J.R. Beauchamp, C.N. Pagel, M. Peckham, P. Ataliotis, P.S. Jat, M.D. Noble, K. Farmer, T.A. Patridge, Myogenic cell lines derived from transgenic moce carrying a thermolabile T antigen: a model system for the derivation of tissue-specific and mutation-specific cell lines, Dev. Biol. 162 (1994) 486-498.

24. C. Brun, D. Suter, C. Pauli, P. Dunant, H..Lochmüller J.M. Burgunder, D. Schümperli, J. Weis, U7 snRNAs induce correction of mutated dystrophin pre-mRNA by exon skipping, Cellular Molec. Life Sci. 60 (2003)557-566.

25. L.H. Jørgensen, N. Larochelle, K. Orlopp, P. Dunant, R.W. Dudley, R. Stucka, C. Thirion, M.C. Walter, S.H. Laval, H. Lochmuller, Efficient and fast functional screening of microdystrophin constructs in vivo and in vitro for therapy of Duchenne muscular dystrophy, Hum. Gene. Ther. 20 (2009) 641-650.

26. A. Musarò, L. Barberi, Isolation and culture of mouse satellite cells, Methods Mol. Biol. 633 (2010) 101-111. doi: 10.1007/978-1-59745-019-5_8.

27. Andrews S. (2010). FastQC: a quality control tool for high throughput sequence data. http://www.bioinformatics.babraham.ac.uk/projects/fastqc.

28. Krueger F., 2012. Trim Galore! A quality trimming tool for high throughput sequence data. https://www.bioinformatics.babraham.ac.uk/projects/trim_galore/

29. A. Dobin, C.A. Davis, F. Schlesinger, J. Drenkow, C. Zaleski, S. Jha, P. Batut, M. Chaisson, T.R. Gingeras, STAR: ultrafast universal RNA-seq aligner, Bioinformatics, 29 (2013) 15-21.

30. Love M.I., Huber W., Anders S., 2014. "Moderated estimation of fold change and dispersion for RNA-seq data with DESeq2." Genome Biology, 15, 550. doi: 10.1186/s13059-014-0550-8]

31. R Core Team, 2017. R: A language and environment for statistical computing. R Foundation for Statistical Computing, Vienna, Austria. URL https://www.R-project.org/.

32. Lawrence M., Huber W., Pagès H., Aboyoun P., Carlson M., Gentleman R., Morgan M.T., Carey V.J., 2013. Software for computing and annotating genomic ranges. PLOS Comput. Biol. 9, e1003118

33. Y. Benjamini, Y. Hochberg, Controlling the False Discovery Rate: A Practical and Powerful Approach to Multiple Testing, Journal of the Royal Statistical Society. Series B (Methodological), 57 (1995) 289–300. JSTOR, www.jstor.org/stable/2346101

34. G. Yu, L.G. Wang, Y. Han, Q.Y. He, clusterProfiler: an R package for comparing biological themes among gene clusters, OMICS: A Journal of Integrative Biology 16 (2012) 284-287. doi: 10.1089/omi.2011.0118.

35. G. Grynkiewicz, M. Poenie, R.Y. Tsien, A new generation of Ca2+ indicators with greatly improved fluorescence properties, J. Biol. Chem. 260 (1985) 3440-3450.

36. R.C. Choi, G.K. Chu, N.L. Siow, A.W. Yung, L.Y. Yung, P.S. Lee, C.C. Lo, J. Simon, T.T. Dong, E.A. Barnard, K.W. Tsim, Activation of UTP-Sensitive P2Y2 Receptor Induces the Expression of Cholinergic Genes in Cultured Cortical Neurons: A Signaling Cascade Triggered by Ca2+ Mobilization and Extracellular Regulated Kinase Phosphorylation, Mol. Pharm. 84 (2013) 50-61. DOI: https://doi.org/10.1124/mol.112.084160;

37. L. Wang, M. Andersson, L. Karlsson, M-A. Watson, D.J. Cousens, S. Jern, D. Erlinge, Increased Mitogenic and Decreased Contractile P2 Receptors in Smooth Muscle Cells by Shear Stress in Human Vessels With Intact Endothelium, Arteriosclerosis, Thrombosis, and Vascular Biology, 23 (2003) 1370-1376.

38. G. Nylund, L. Hultman, S. Nordgren, D.S. Delbro P2Y2- and P2Y4 purinergic receptors are over-expressed in human colon cancer. Auton Autacoid Pharmacol. 27 (2007) 79-84.

39. Vázquez-Cuevas F.G., Zárate-Díaz E.P., E. Garay, R.O., Arellano, 2010. Functional expression and intracellular 18ignalling of UTP-sensitive P2Y receptors in theca-interstitial cells, Reprod Biol Endocrinol. 2010 Jul 8 (2010):88. doi: 10.1186/1477-7827-8-88.

40. V. Salvestrini, R. Zini, L. Rossi, S. Gulinelli, R. Manfredini, E. Bianchi, W. Piacibello, L. Caione, G. Migliardi, M.R. Ricciardi, A. Tafuri, M. Romano, S. Salati, F. Di Virgilio, S. Ferrari, M. Baccarani, D. Ferrari, R.M. Lemoli, Purinergic signaling inhibits human acute myeloblastic leukemia cell proliferation, migration, and engraftment in immunodeficient mice. Blood 119 (2012) 217-226. doi: 10.1182/blood-2011-07-370775.

41. Y.V. Evtodienko, V.V. Teplova, J. Duszyński, L. Wojtczak, Effect of cyclosporin A on Ca^{2+} fluxes and the rate of respiration in Ehrlich ascites tumour cells, Biochem. Mol. Biol. Int. 35 (1995)1113–1121.

42. G Burnstock, TR Arnett, IR Orriss, Purinergic signalling in the musculoskeletal system, Purinergic Signal. 9 (2013) 541-572. doi: 10.1007/s11302-013-9381-4.

43. W. Banachewicz, D. Supłat, P. Krzemiński, P. Pomorski, J. Barańska, P2 nucleotide receptors on C2C12 satellite cells, Purinergic Signal. 1 (2005) 249-257. doi: 10.1007/s11302-005-6311-0.

44. R. Araya, M.A. Riquelme, E. Brandan, J.C. Sáez, The formation of skeletal muscle myotubes requires functional membrane receptors activated by extracellular ATP, Brain Res. Brain Res. Rev. 47 (2004) 174-188.

45. C.N.J. Young, N. Chira, J. Róg, R. Al-Khalidi, M. Benard, L. Galas, P. Chan, D. Vaudry, K Zabłocki, D.C. Górecki, Sustained activation of P2X7 induces MMP-2-evoked cleavage and functional purinoceptor inhibition J. Mol. Cell Biol. 10 (2018) 229-242. doi: https://doi.org/10.1093/jmcb/mjx030.

46. 44. D.S. Delbro, G. Nylund, S. Nordgren, Demonstration of P2Y4 purinergic receptors in the HT-29 human colon cancer cell line, Auton. Autacoid Pharmacol. 25 (2005) 163-166.

Figure legends

Fig 1. RNAseq analysis in myoblasts derived from w/t and mdx mice

A: *Hierarchical clustering of the normalised read counts across all genes identifies clear discrimination between the dystrophic (mdx) and control (w/t) cells. Cell colour represents the dissimilarity between samples, with dark blue indicating no difference.*
B: Volcano plot showing the results of the differential expression analyses across all genes, with the (-log10) adjusted p value on the y-axis representing the significance of the change, and the log2 fold change on the x-axis representing the magnitude of the change. Genes are classed as showing significant differential expression with fold change greater than 2-fold (up or down) with an adjusted p-value less than 0.05. In addition, the expression must show FPKM greater than 1 in at least one of the two conditions. Significantly upregulated (red) and downregulated (blue) genes between the mdx (SC5) and control (IMO) cells are highlighted

Fig. 2 Heatmap of genes encoding members of the purinoceptor ATP receptor family

Variance stabilisation transformed read counts were normalised such that each row had mean 0 and standard deviation 1, such that differences between the mdx and w/t cells could be identified, with downregulated genes highlighted blue and upregulated genes highlighted red.

Fig. 3 Effect of ATP, UTP and AR-C118925XX on Ca^{2+} release from the ER stores in myoblasts measured in the absence of extracellular calcium
A, effect of ATP. Traces from one representative experiment out of three.
B, Mean values collected from three experiments ± S.D. Asterisks refer to statistically significant differences, as follows:

*mdx vs w/t (500 μM ATP) *p<0.029;*
*mdx vs w/t (1 mM ATP) * p<0.027;*
*mdx vs mdx + 10 μM AR-C118925XX (500 μM ATP) * p<0.044;*
*mdx vs mdx +10 μM AR-C118925XX (1 mM ATP) * p<0.030;*
C, effect of UTP. Traces from one representative experiment out of five.
D, Mean values collected from five experiments ± S.D. Asterisks refer to statistically significant differences, as follows:
*mdx vs w/t (100 μM UTP) * p< 0.001;*
*mdx vs w/t (500 μM UTP) * p< 0.001;*
*mdx vs mdx + 10 μM AR-C118925XX (100 μM UTP) * p< 0.0003*
*mdx vs mdx + 10 μM AR-C118925XX (500 μM UTP) *p< 0.001;*

In this experiment fluorescence was measured with the use of Shimadzu spectrofluorospectrometer RF-5301 PC. Dark bars – w/t myoblasts, bright bars – mdx myoblasts.

Fig. 4 P2RY2 and P2RY4 expression in w/t and mdx myoblasts.

*A, Mean values ± S.D. for qPCR for P2RY2 and P2RY4 transcripts. Data collected from six and four experiments, respectively. * p<0.001 . B. Representative Western blots for P2RY2 and P2RY4 and mean values ± S.D. of the relative level of these proteins in mdx myoblasts collected from three and six experiments, respectively. * p<0.02, ** p<0.05.*

Fig. 5 P2RY2 and P2RY4 localization to the plasma membrane

*A, Representative Western blot of P2RY2 and P2RY4 in cell fractions grown under "de-immorto" conditions (as in the entire paper) normalised to Na^+-K^+ATPase. B, Representative Western blot of P2RY2 and P2RY4 in crude homogenate and in the plasma membrane of w/t and mdx myoblasts grown under "immorto" conditions, normalised to caveolin. D, Mean values ± S.D. of Western blot data for P2RY2 normalised to caveolin "in immorto cells" for five independent experiments. E, Mean values ± S.D. of Western blot data for P2RY4 normalised to caveolin in immorto cells for five independent experiments. * p<0.01, ** p<0.02.*

Fig. 6 Immunocytochemical detection of P2RY2 and P2RY4 in w/t and mdx myoblasts

Upper panel: P2RY2. Increased amount of P2RY2 protein in a whole cell but particularly in the plasma membrane. Lower panel: P2RY4. Increased total amount of P2RY4 with perinuclear localization in particular. Bar = 10 μM

Fig. 7 Effect of P2Y2 gene silencing on UTP-evoked Ca2+ release from the ER stores in myoblasts measured in the absence of extracellular calcium

Illustrative Western blot confirming an efficient silencing of the P2RY2 gene and nucleotide–induced Ca^{2+} trace obtained in the same experiment. In this experiment fluorescence was measured with the use of Hitachi fluorescence spectrophotometer F 7000.

Fig. 8 Effect of UTP and AR-C118925XX on cell motility

Myoblasts motility (cell path length) expressed in micrometers. Data collected from 3-5 independent experiment.

mdx unstimulated vs w/t unstimulated p<0.014 n=5;

mdx stimulated with UTP vs mdx unstimulated p<0.03 n=5.

Fig. 9: Heatmap showing expression levels for genes associated with calcium ion homeostasis

It is based on gene ontology terms calcium ion homeostasis (GO:0055074), calcium-mediated signaling (GO:0019722), calcium ion binding (GO:0005509), calcium ion transport (GO:0006816), or calcium channel activity (GO:0005262). Variance stabilisation transformed read counts were normalised such that each row had mean 0 and standard deviation 1, such that differences between the mdx and control (w/t) cells could be identified, with downregulated genes highlighted blue and upregulated genes highlighted red.

Fig. 10 Relative calcium content in the ER and calsequestrin and calreticulin levels in w/t and mdx myoblasts.

*A, Increase of cytosolic Ca^{2+} concentration upon treatment of cells with ionomycin. Mean value of data collected from seven independent experiments ± SD. * p< 0.015.*

*B, calsequestrin and C, calreticulin content in myoblasts. Representative Western blots and mean values ± S.D. collected from seven experiments. *p<0.020*

Fig. 11 Relative amounts of SERCA1 and SERCA 2 in w/t and mdx myoblasts. *Representative Western blot for SERCA1 and mean values ± S.D. of the relative level of these proteins in mdx myoblasts collected from four experiments. *p<0.022.Representative Western blot for SERCA2A and mean values ± S.D. of the relative level of these proteins in mdx myoblasts collected from four experiments. *p<0.006. Representative Western blot for SERCA2B and mean values ± S.D. of the relative level of these proteins in mdx myoblasts collected from four experiments. n.s.*

Fig. 12 Relative amount of protein G11q subunit α and IP3R in wt and mdx myoblasts *A, representative Western blot for Gq_{11} subunit α from one of three independent experiments, and mean values of data collected from three experiments. * p<0.047;*
*B, representative Western blot for IP3R from one of three independent experiments, and mean values of data collected from eight experiments. * p<0.016;*

Fig. 13 Relative amount of protein PLC isoforms 1-4 in w/t and mdx myoblasts. *Each panel shows one representative Western blot out of four independent experiments and a mean values ± S.D of collected Western blot data. A, PLCβ1 n=4 $p \leq 0.29$; B, PLCβ2 n=4 $p \leq 0.552$; C, PLCβ3 n=4 $p \leq 0.006$; PLCβ4 n=3 $p \leq 0.004$.*

Fig. 14 Relative amount of PMCA protein and NCX isoforms 1 and 3 in w/t and mdx myoblasts.
Each panel shows one representative Western blot out of an indicated below number of independent experiments and a mean values ± S.D of collected Western blot data. A, PMCA n=6 $p \leq 0.04$; B, NCX1 n=3 $p \leq 0.046$; C, NCX3 n=4 $p \leq 0.016$.

Fig. 15 General scheme showing summarised results of our investigations concerning aberrant calcium homeostasis in mdx myoblasts.
Left site presents data shown in this paper while on the right there are results of our previous study. Red characters or arrows mean increased protein levels or stimulated processes, respectively. Green - decreased proteins levels. Black – unchanged or not determined.

Suppl. Fig. 1. Effect of ATP, UTP on cytosolic calcium concentration in w/t and mdx myoblasts measured in the presence of extracellular calcium.

A, Effect of 500 μM ATP; B, effect of 100 μM UTP. $[Ca^{2+}]c$ was measured with Fura2-AM in the presence of 2 mM $CaCl_2$ in the extracellular solution. Figures shows representative traces out of 7 experiments for cells grown under "de-immortalizing" conditions as those applied in other experiments shown in this paper. Similar effects have been obtained in myoblasts grown under immortalizing conditions. In this experiment fluorescence was

measured with the use of Hitachi fluorescence spectrophotometer F 7000. Substantially higher elevation of [Ca2+]c in cells excited with ATP than with UTP reflects simultaneous ATP-evoked stimulation of metabotropic and ionotropic receptors (P2RY and P2RX, respectively). In this experiment fluorescence was measured with the use of Hitachi fluorescence spectrophotometer F 7000.

Suppl. ***Fig. 2 Effect of ATP and AR-C118925XX on Ca^{2+} release from the ER stores in myoblasts measured in the absence of extracellular calcium***

Upper panel: effect of ATP at various concentrations. Mean values collected from five experiments ± S.D.

*mdx vs w/t with 100 μM ATP * p<0.026,*
*mdx vs w/t with 500 μM ATP * p<0.0001*
*mdx vs w/t with 1 mM ATP * p<0.0001;*

Lower panel: effect of ATP and P2RY2 antagonist (AR-C118925XX) . Asterisks refer to statistically significant differences, as follows:
*w/t vs. w/t + 10 μM AR-C118925XX 500 μM ATP *p<0.0003;*
*w/t vs. w/t +10 μM AR-C118925XX 1 mM ATP * p<0.0005;*
*mdx vs mdx + 3 μM AR-C118925XX 500 μM ATP * p<< 0.0001;*
*mdx vs mdx + 10 μM AR-C118925XX 500 μM ATP * p<< 0.0001*
*mdx vs mdx + 3 μM AR-C118925XX 1 mM ATP * p<< 0.0001;*
*mdx vs mdx + 10 μM AR-C118925XX 1 mM ATP * p<< 0.0001*

Fluorescence (Fura-2) was measured with the use of Shimadzu spectrofluorospectrometer RF-5301 PC. Dark dots – w/t myoblasts, bright dots – mdx myoblasts.

Suppl. ***Fig. 3 Effect of UTP and AR-C118925XX on Ca^{2+} release from the ER stores in myoblasts measured in the absence of extracellular calcium***

Upper panel: effect of UTP at various concentrations. Mean values collected from five experiments ± S.D. Asterisks refer to statistically significant differences, as follows:

*mdx vs w/t with 100 μM UTP * p<<0.0001;*
*mdx vs w/t with 500 μM UTP * p<<0.0001*
*mdx vs w/t with 1 mM UTP * p<<0.0001;*
Lower panel: effect of UTP and P2RY2 antagonist (AR-C118925XX) .
*w/t vs. w/t + 10 μM AR-C118925XX 100 μM UTP * p<0.002;*
*w/t vs. w/t + 10 μM AR-C118925XX 500 μM UTP * p<0.023;*
*mdx vs mdx + 3 μM AR-C118925XX 100 μM ATP * p<< 0.0001;*
*mdx vs mdx + 10 μM AR-C118925XX 100 μM ATP * p<< 0.0001*

Fura-2 fluorescence was measured with the use of Shimadzu spectrofluorospectrometer RF-5301 Dark dots – w/t myoblasts, bright dots – mdx myoblasts.

Suppl. Fig 4. Representative Western blot of P2RY2 and P2RY4 in the plasma membrane of cells grown under "immorto" conditions

*A Representative Western blot of P2RY2 and P2RY4 in crude homogenate and in the plasma membrane of w/t and mdx myoblasts grown under normalised to caveolin. B, Mean values ± S.D. of Western blot data for P2RY2 normalised to caveolin for five independent experiments. E, Mean values ± S.D. of Western blot data for P2RY4 normalised to caveolin for five independent experiments. * p<0.01, ** p<0.02.*

Suppl. Fig. 5. Immunocytochemical detection of P2RY2 and P2RY4 in w/t and mdx myoblasts grown under "immorto" conditions

Upper panel: P2RY2. Increased amount of P2RY2 protein in a whole cell but particularly in the plasma membrane. Lower panel: P2RY4. Increased total amount of P2RY4 with perinuclear localization in particular. Bar = 10 μM

Suppl. 6 Effect of P2Y2 gene silencing on UTP-evoked Ca^{2+} release from the ER stores in myoblasts measured in the absence of extracellular calcium

Cells were grown under "immorto" conditions. Representative UTP–induced Ca^{2+} trace. In this experiment fluorescence was measured with the use of Hitachi fluorescence spectrophotometer F 7000.

Fig. 1

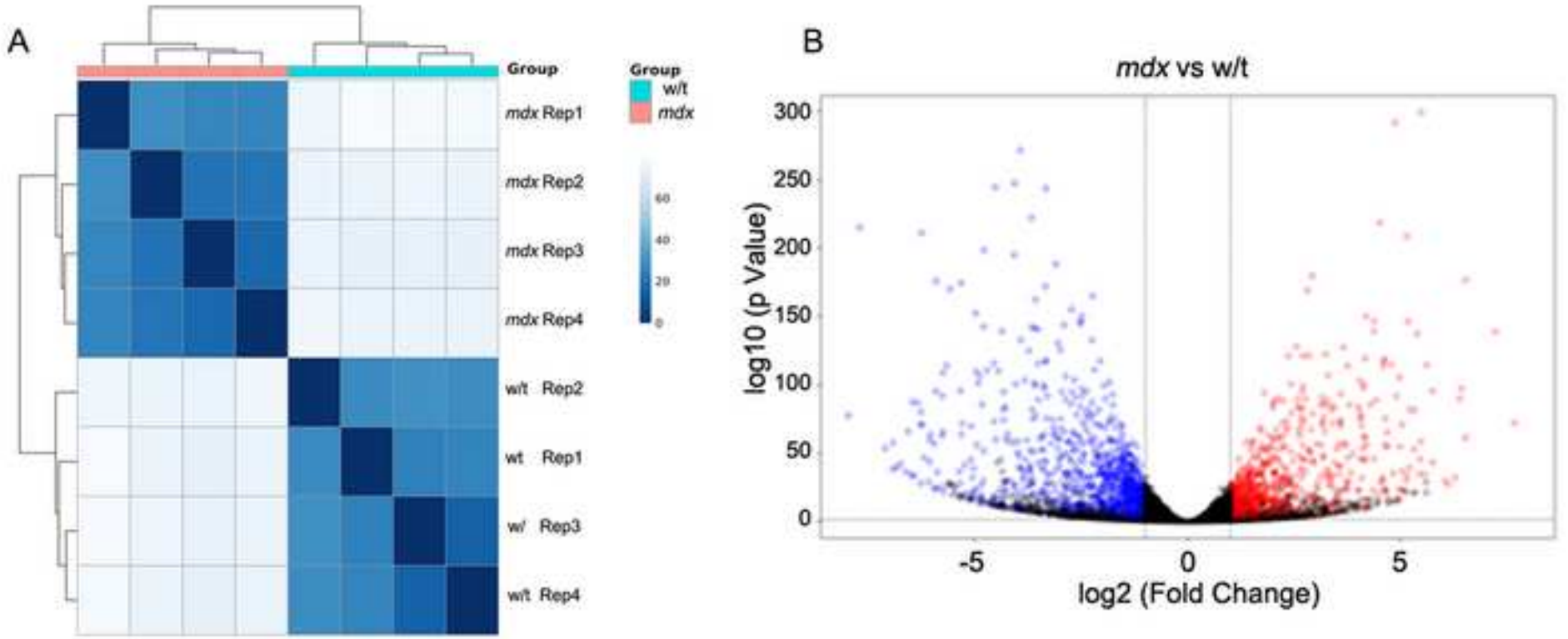
A
Group
Group
w/t
mdx
mdx Rep1
mdx Rep2
mdx Rep3
mdx Rep4
w/t Rep2
wt Rep1
w/ Rep3
w/t Rep4
60
40
20
0
B
mdx vs w/t
log10 (p Value)
300
250
200
150
100
50
0
-5
0
5
log2 (Fold Change)

Fig. 2

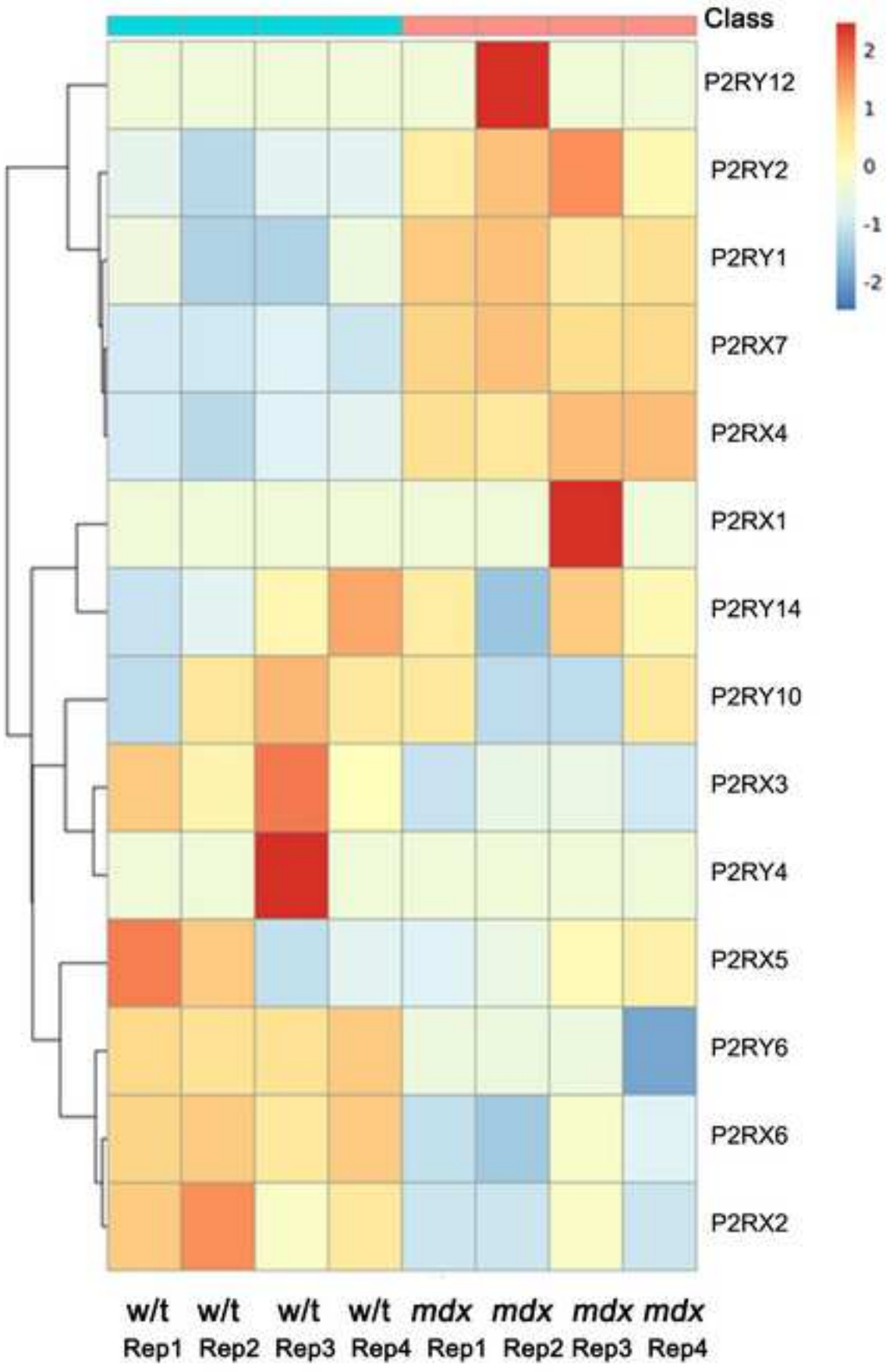
Class
2
1
0
-1
-2
P2RY12
P2RY2
P2RY1
P2RX7
P2RX4
P2RX1
P2RY14
P2RY10
P2RX3
P2RY4
P2RX5
P2RY6
P2RX6
P2RX2
w/t Rep1
w/t Rep2
w/t Rep3
w/t Rep4
mdx Rep1
mdx Rep2
mdx Rep3
mdx Rep4

Fig. 3

A

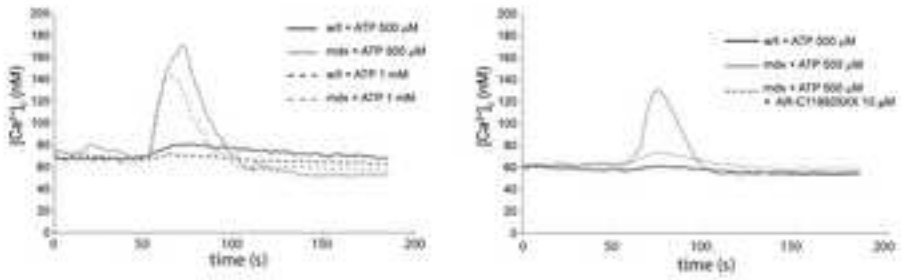
time (s)
time (s)

B

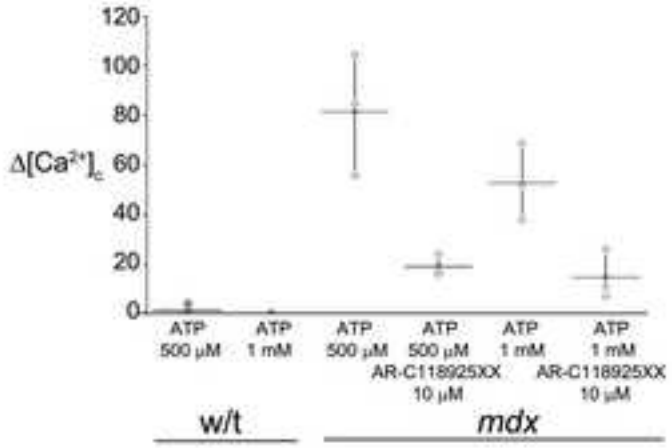
Δ[Ca2+]c
ATP 500 µM
ATP 1 mM
ATP 500 µM
ATP 500 µM AR-C118925XX 10 µM
ATP 1 mM
ATP 1 mM AR-C118925XX 10 µM
w/t
mdx

C

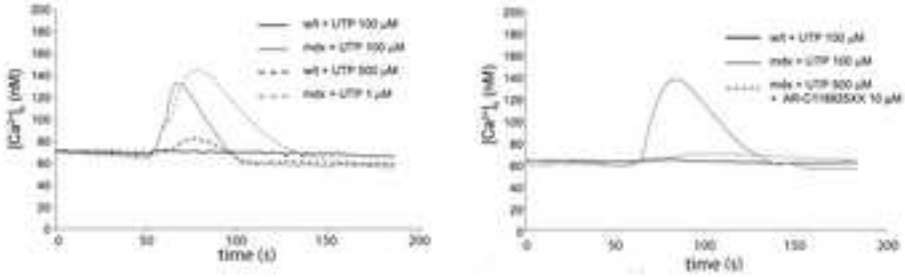
time (s)
time (s)

D

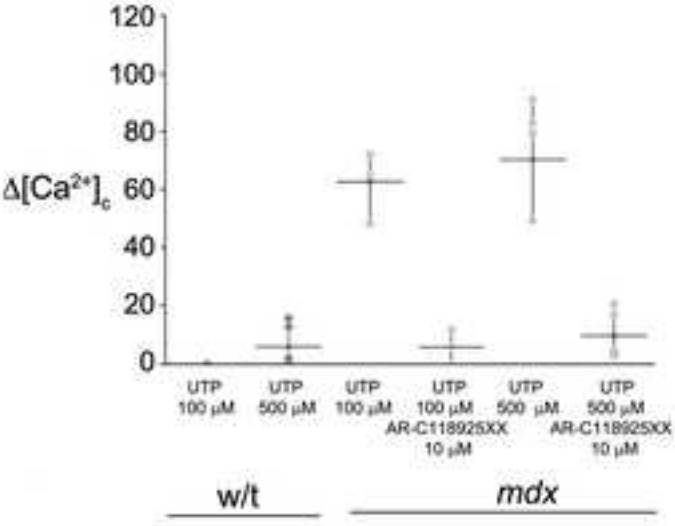
Δ[Ca2+]c
UTP 100 µM
UTP 500 µM
UTP 100 µM
UTP 100 µM AR-C118925XX 10 µM
UTP 500 µM
UTP 500 µM AR-C118925XX 10 µM
w/t
mdx

Fig.4

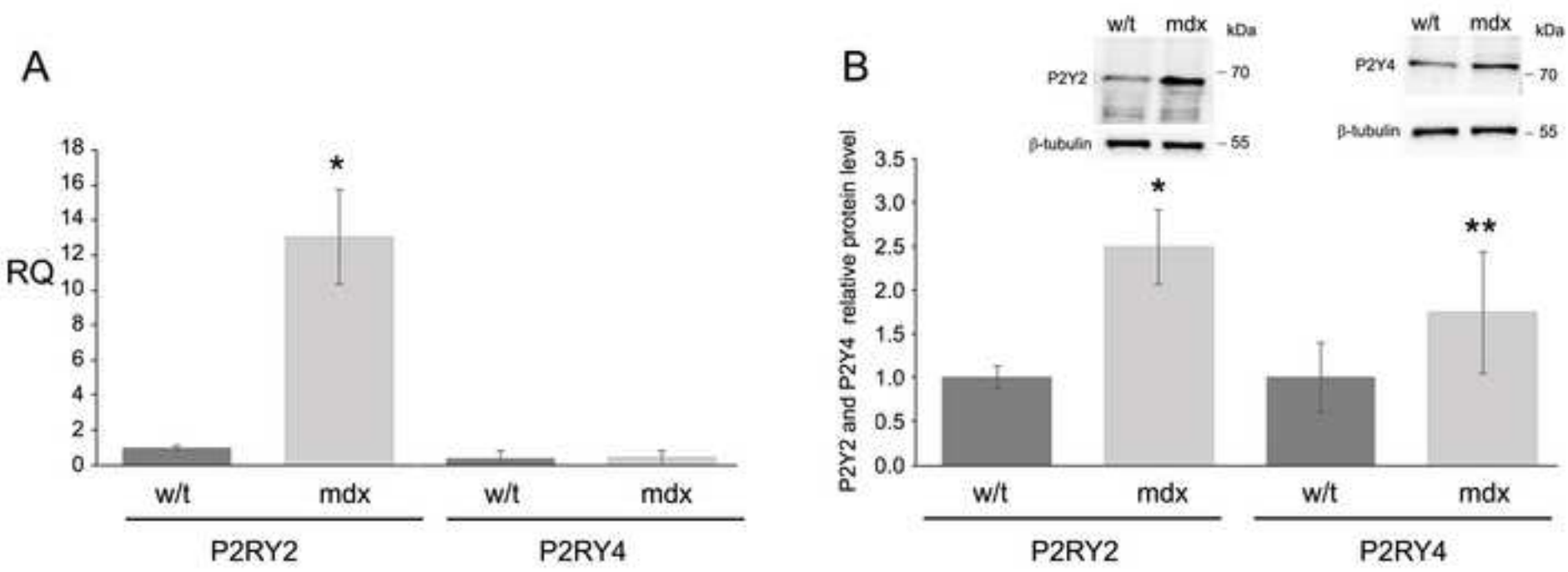
A
RQ
18
16
14
12
10
8
6
4
2
0
*
w/t
mdx
w/t
mdx
P2RY2
P2RY4
B
w/t
mdx
kDa
P2Y2
70
β-tubulin
55
w/t
mdx
kDa
P2Y4
70
β-tubulin
55
P2Y2 and P2Y4 relative protein level
3.5
3.0
2.5
2.0
1.5
1.0
0.5
0.0
*
**
w/t
mdx
w/t
mdx
P2RY2
P2RY4

Fig. 5

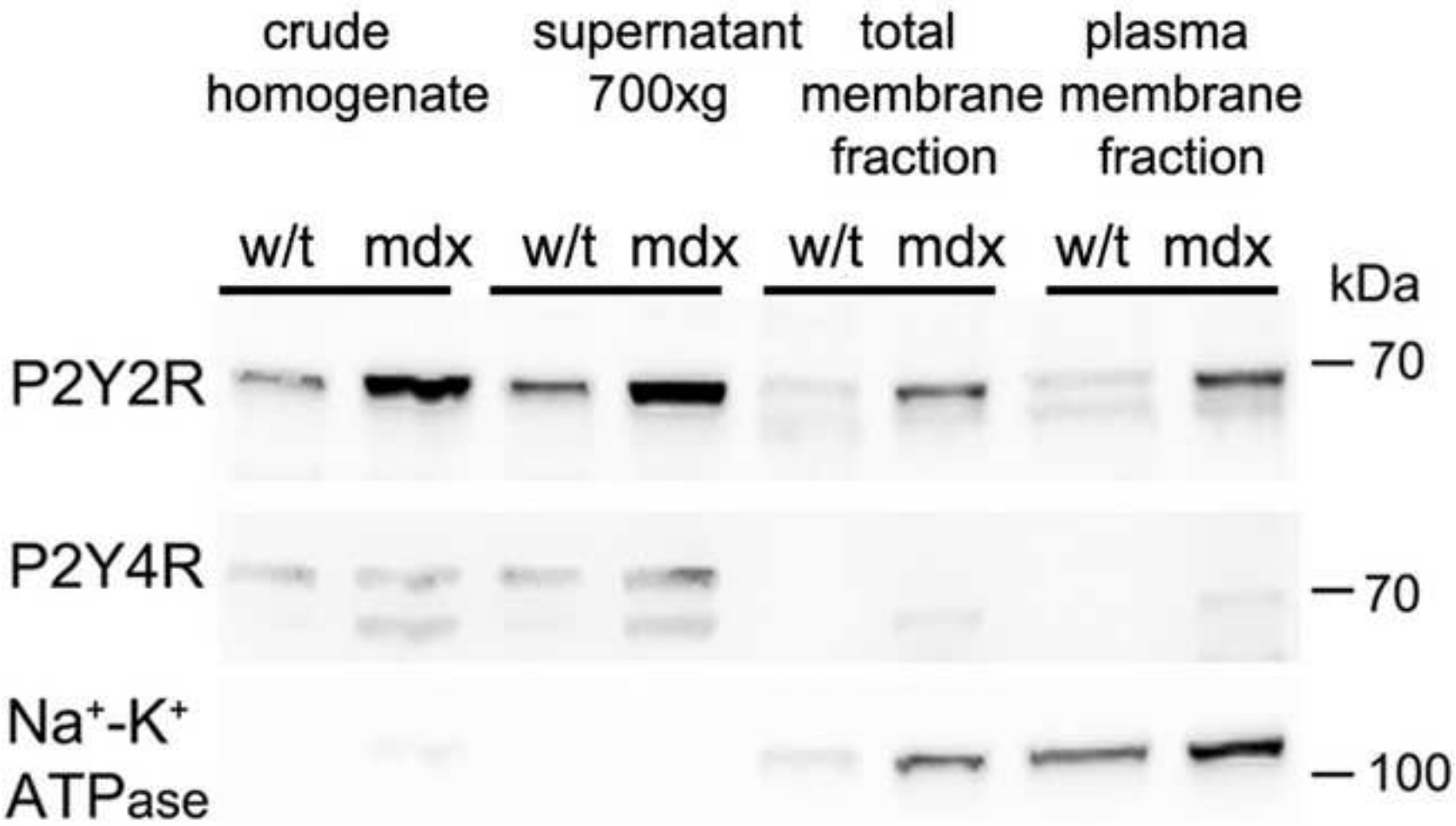
crude homogenate
supernatant 700xg
total membrane fraction
plasma membrane fraction
w/t
mdx
w/t
mdx
w/t
mdx
w/t
mdx
kDa
P2Y2R
70
P2Y4R
70
Na+-K+ ATPase
100

Fig. 6

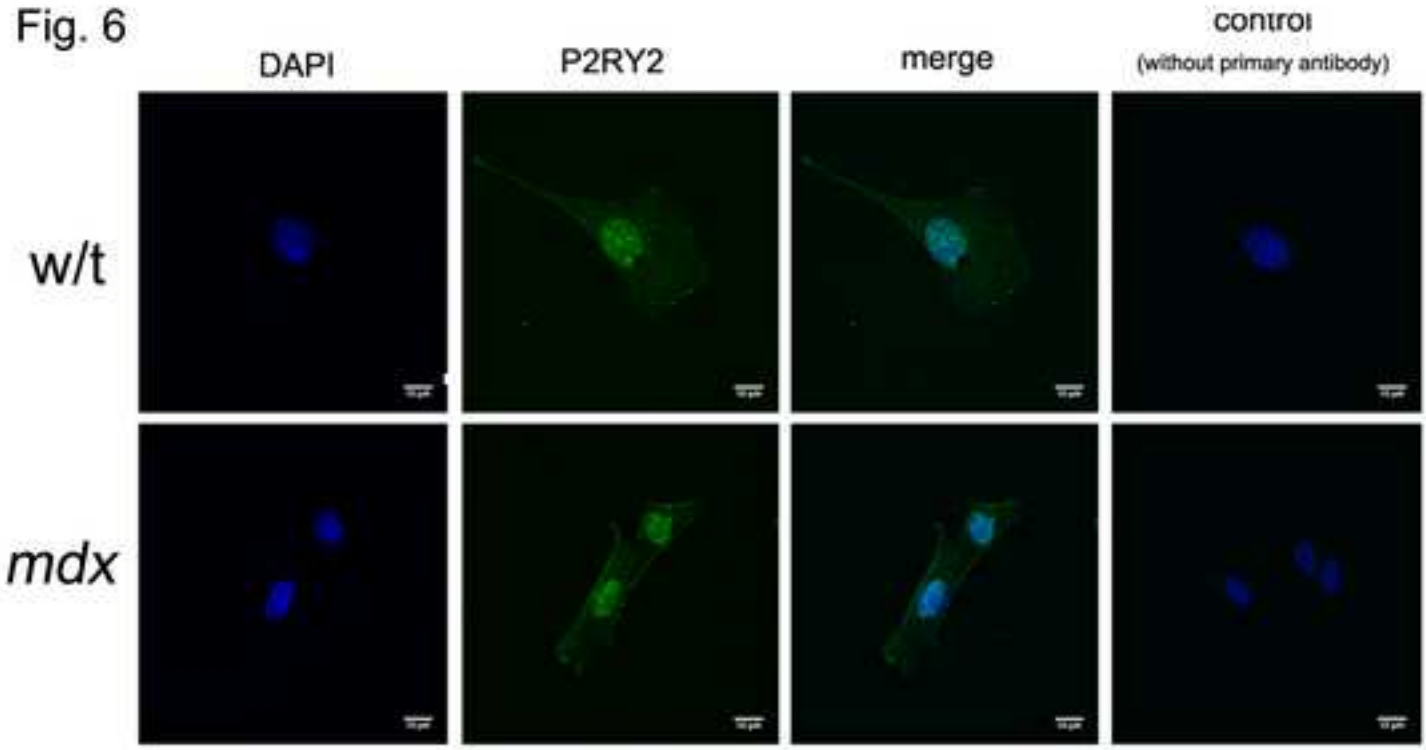
DAPI
P2RY2
merge
control
(without primary antibody)
w/t
mdx

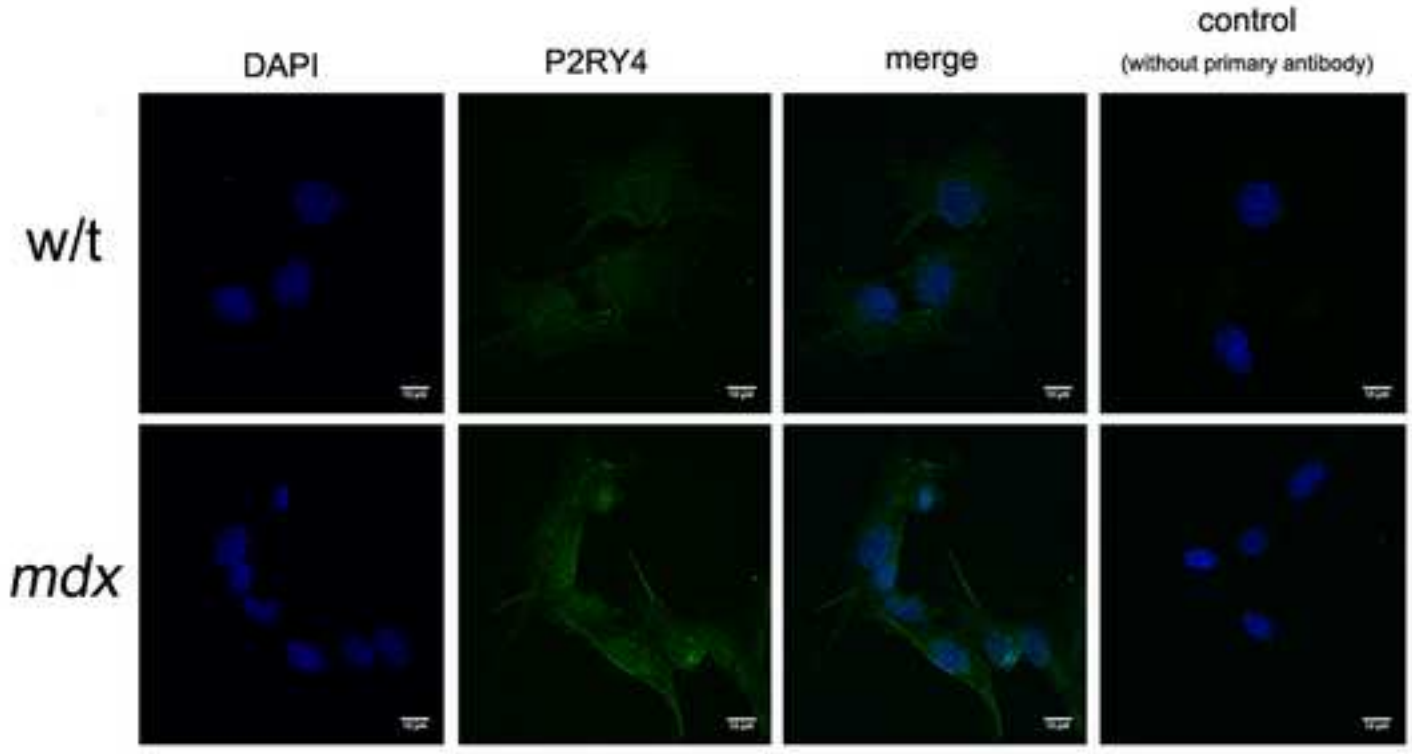
DAPI
P2RY4
merge
control
(without primary antibody)
w/t
mdx

Fig. 7

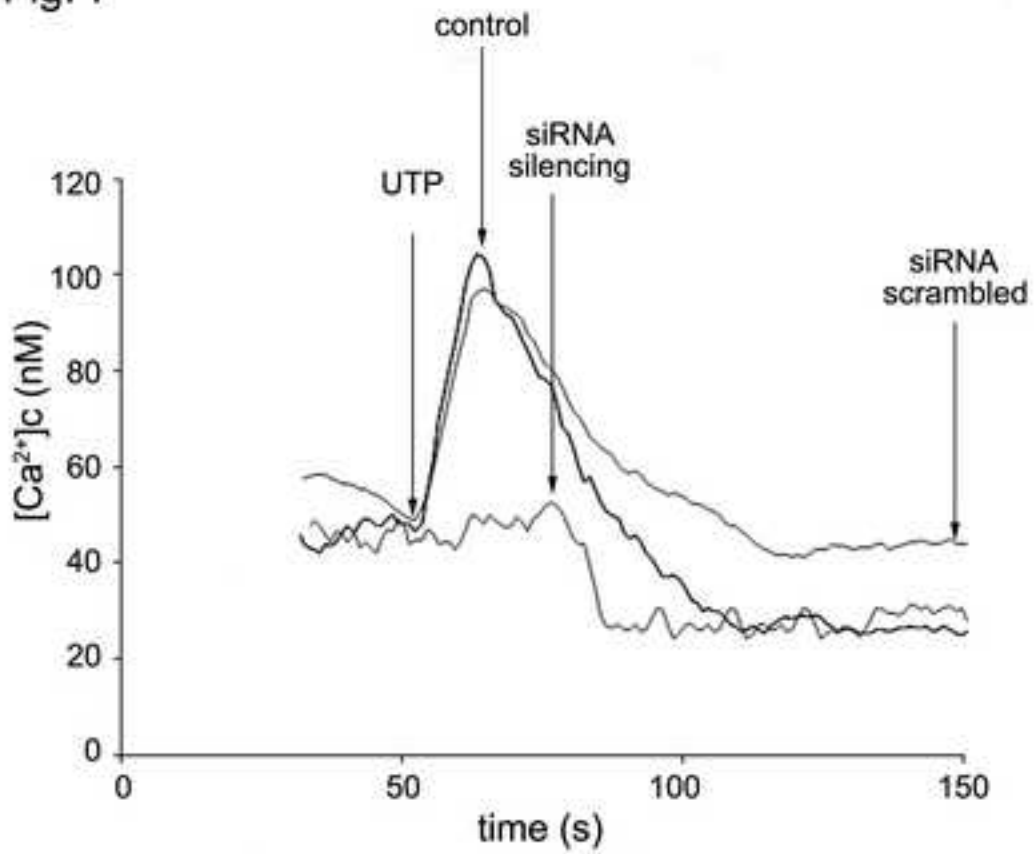
control
siRNA
silencing
UTP
siRNA
scrambled
120
100
80
60
40
20
0
[Ca2+]c (nM)
0
50
100
150
time (s)

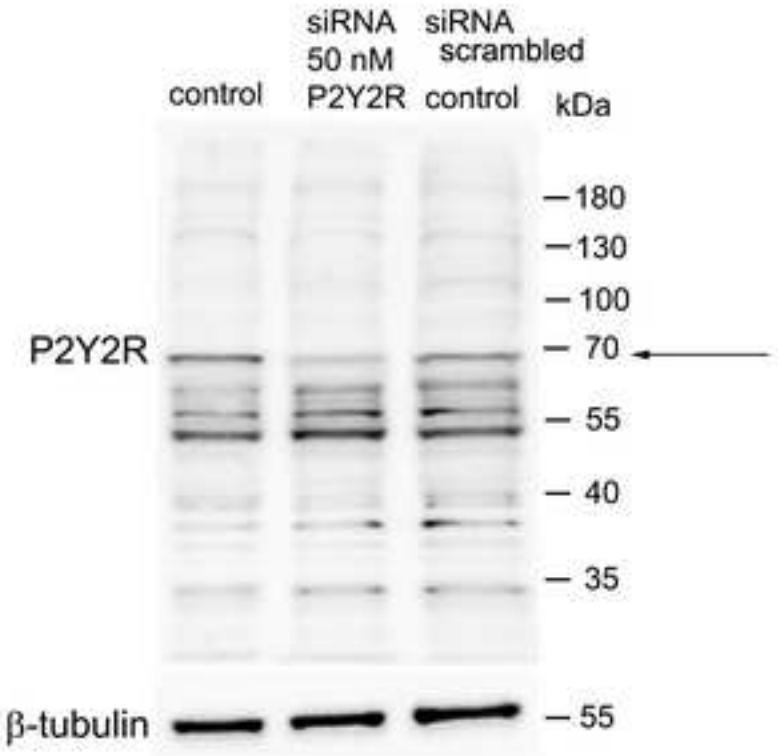
siRNA
50 nM
P2Y2R
siRNA
scrambled
control
control
kDa
180
130
100
70
55
40
35
P2Y2R
β-tubulin
55

Fig. 9

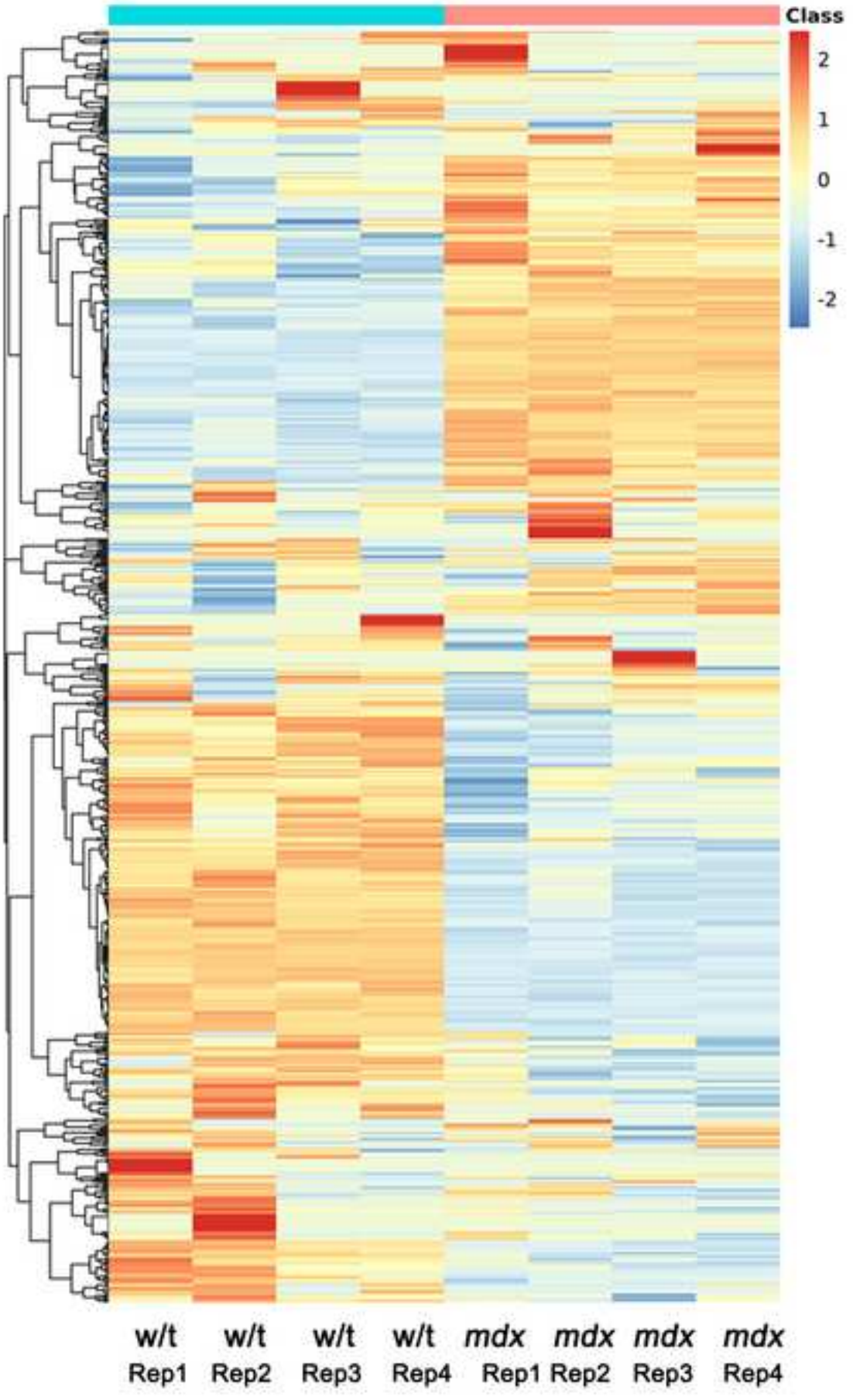
Class
2
1
0
-1
-2
w/t Rep1
w/t Rep2
w/t Rep3
w/t Rep4
mdx Rep1
mdx Rep2
mdx Rep3
mdx Rep4

Fig. 10

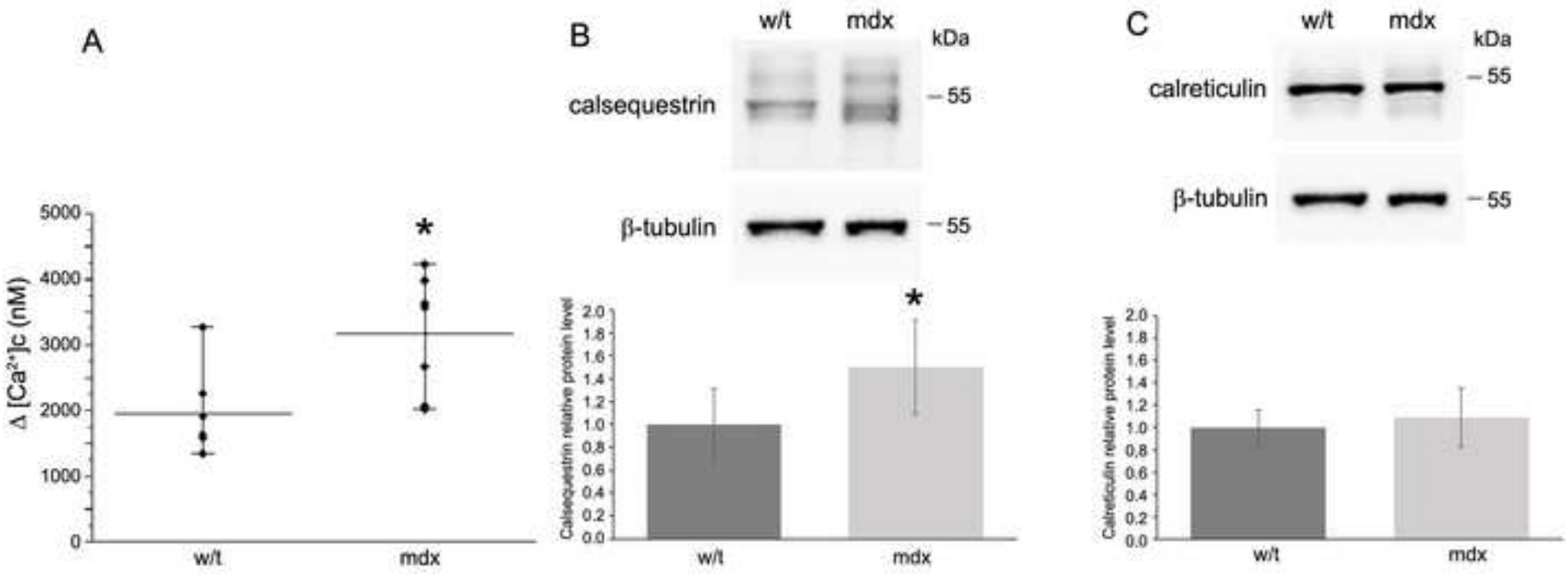
A
Δ [Ca2+]c (nM)
5000
4000
3000
2000
1000
0
*
w/t
mdx
B
w/t
mdx
kDa
calsequestrin
55
β-tubulin
55
Calsequestrin relative protein level
2.0
1.8
1.6
1.4
1.2
1.0
0.8
0.6
0.4
0.2
0.0
*
w/t
mdx
C
w/t
mdx
kDa
calreticulin
55
β-tubulin
55
Calreticulin relative protein level
2.0
1.8
1.6
1.4
1.2
1.0
0.8
0.6
0.4
0.2
0.0
w/t
mdx

Fig. 11

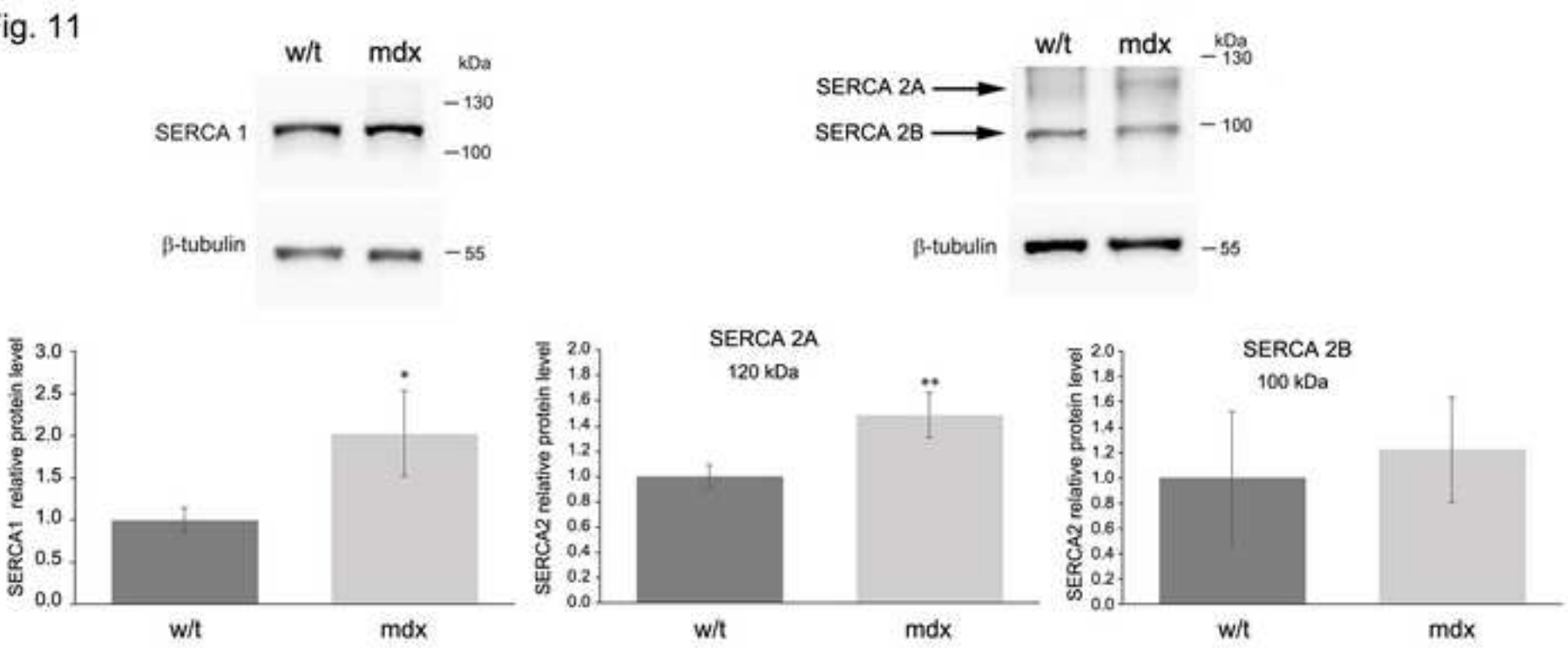
w/t
mdx
kDa
SERCA 1
130
100
β-tubulin
55
SERCA 2A
SERCA 2B
SERCA1 relative protein level
SERCA2 relative protein level
SERCA 2A
120 kDa
SERCA 2B
100 kDa
*
**

Fig. 12

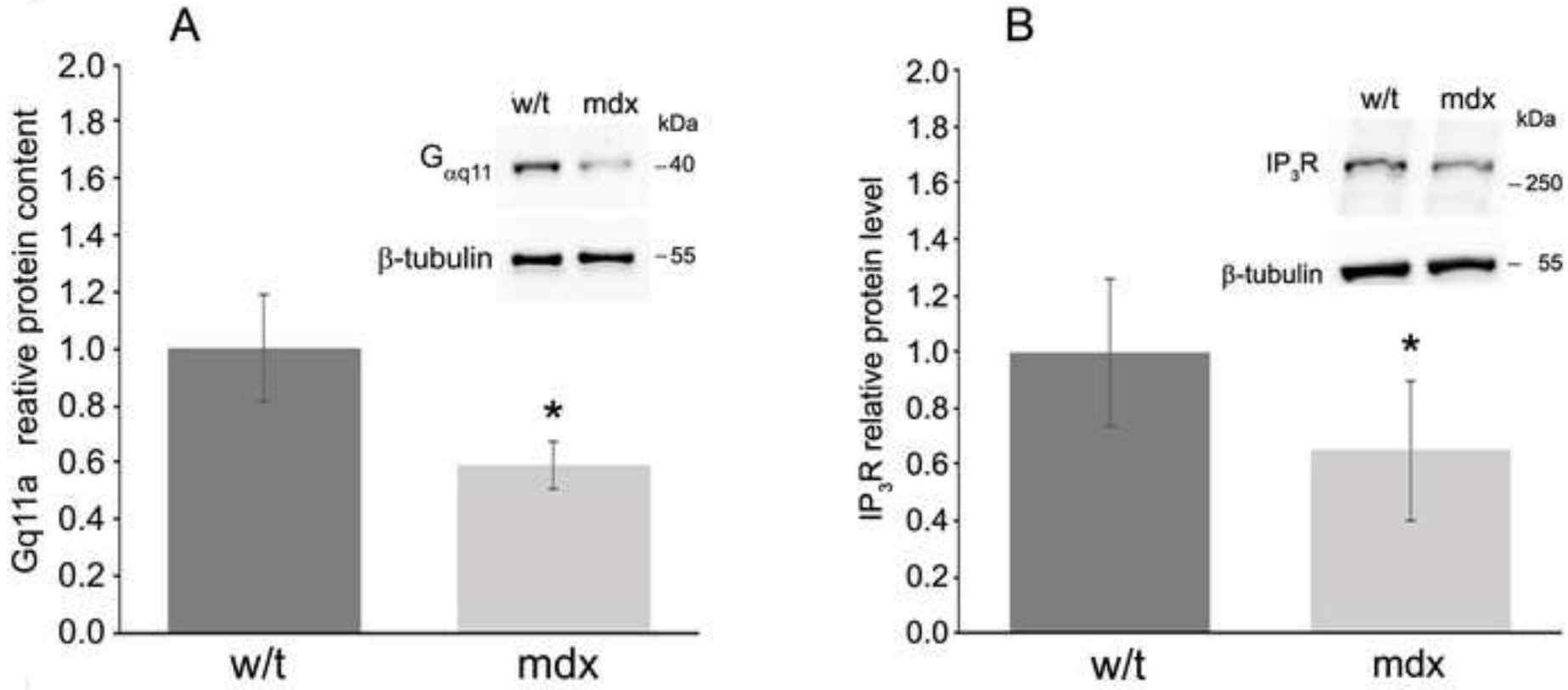
A
Gq11a reative protein content
2.0
1.8
1.6
1.4
1.2
1.0
0.8
0.6
0.4
0.2
0.0
w/t
mdx
*
w/t
mdx
kDa
Gαq11
-40
β-tubulin
-55
B
IP3R relative protein level
2.0
1.8
1.6
1.4
1.2
1.0
0.8
0.6
0.4
0.2
0.0
w/t
mdx
*
w/t
mdx
kDa
IP3R
-250
β-tubulin
- 55

Fig. 13

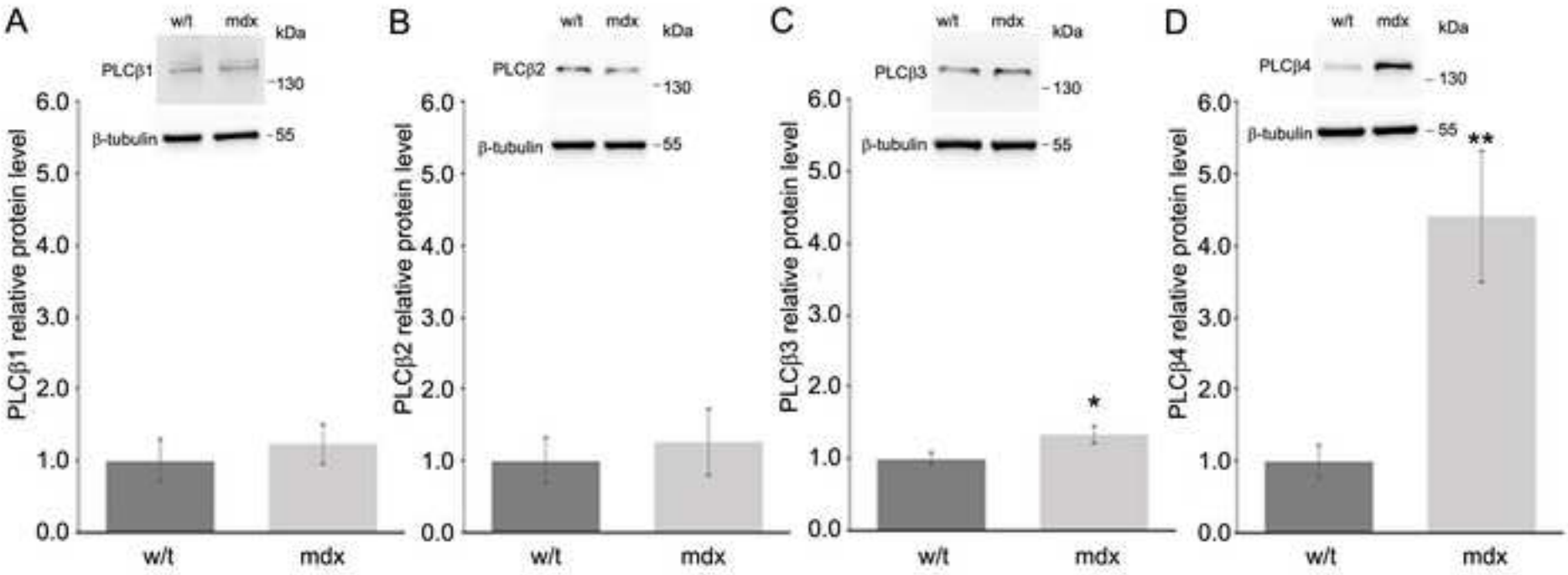
A
w/t
mdx
kDa
PLCβ1
130
β-tubulin
55
PLCβ1 relative protein level
6.0
5.0
4.0
3.0
2.0
1.0
0.0
w/t
mdx
B
w/t
mdx
kDa
PLCβ2
130
β-tubulin
55
PLCβ2 relative protein level
6.0
5.0
4.0
3.0
2.0
1.0
0.0
w/t
mdx
C
w/t
mdx
kDa
PLCβ3
130
β-tubulin
55
PLCβ3 relative protein level
*
6.0
5.0
4.0
3.0
2.0
1.0
0.0
w/t
mdx
D
w/t
mdx
kDa
PLCβ4
130
β-tubulin
55
**
PLCβ4 relative protein level
6.0
5.0
4.0
3.0
2.0
1.0
0.0
w/t
mdx

Fig. 14

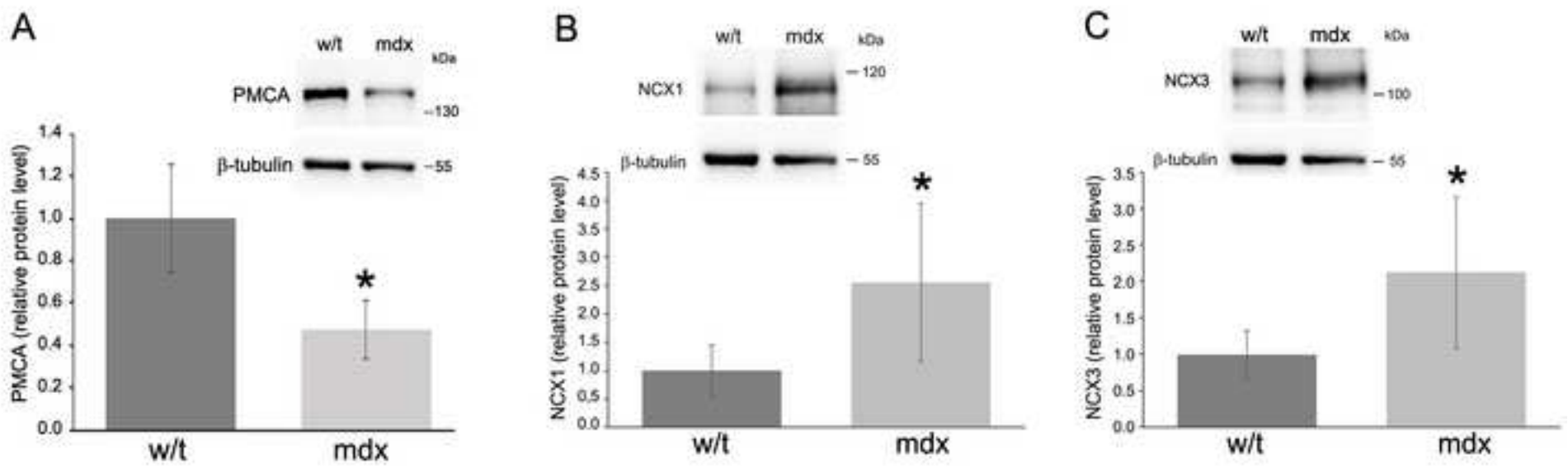
A
w/t
mdx
kDa
PMCA
130
β-tubulin
55
PMCA (relative protein level)
1.4
1.2
1.0
0.8
0.6
0.4
0.2
0.0
*
w/t
mdx
B
w/t
mdx
kDa
NCX1
120
β-tubulin
55
NCX1 (relative protein level)
4.5
4.0
3.5
3.0
2.5
2.0
1.5
1.0
0.5
0.0
*
w/t
mdx
C
w/t
mdx
kDa
NCX3
100
β-tubulin
55
NCX3 (relative protein level)
3.5
3.0
2.5
2.0
1.5
1.0
0.5
0.0
*
w/t
mdx

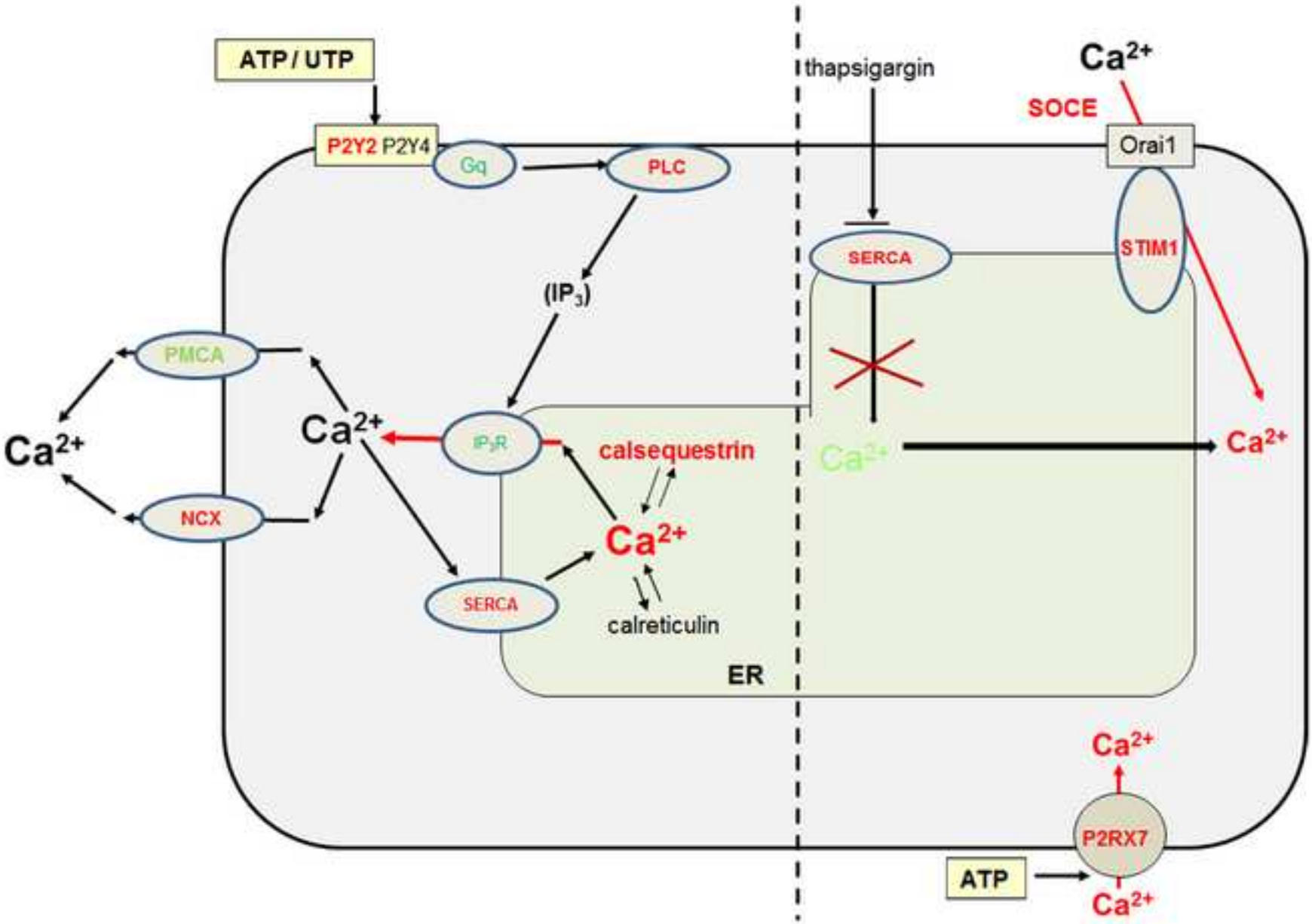
ATP / UTP
P2Y2 P2Y4
Gq
PLC
(IP3)
PMCA
Ca2+
NCX
Ca2+
IP3R
calsequestrin
Ca2+
SERCA
calreticulin
ER
thapsigargin
Ca2+
SOCE
Orai1
STIM1
SERCA
Ca2+
Ca2+
Ca2+
P2RX7
ATP
Ca2+

Fig. 8

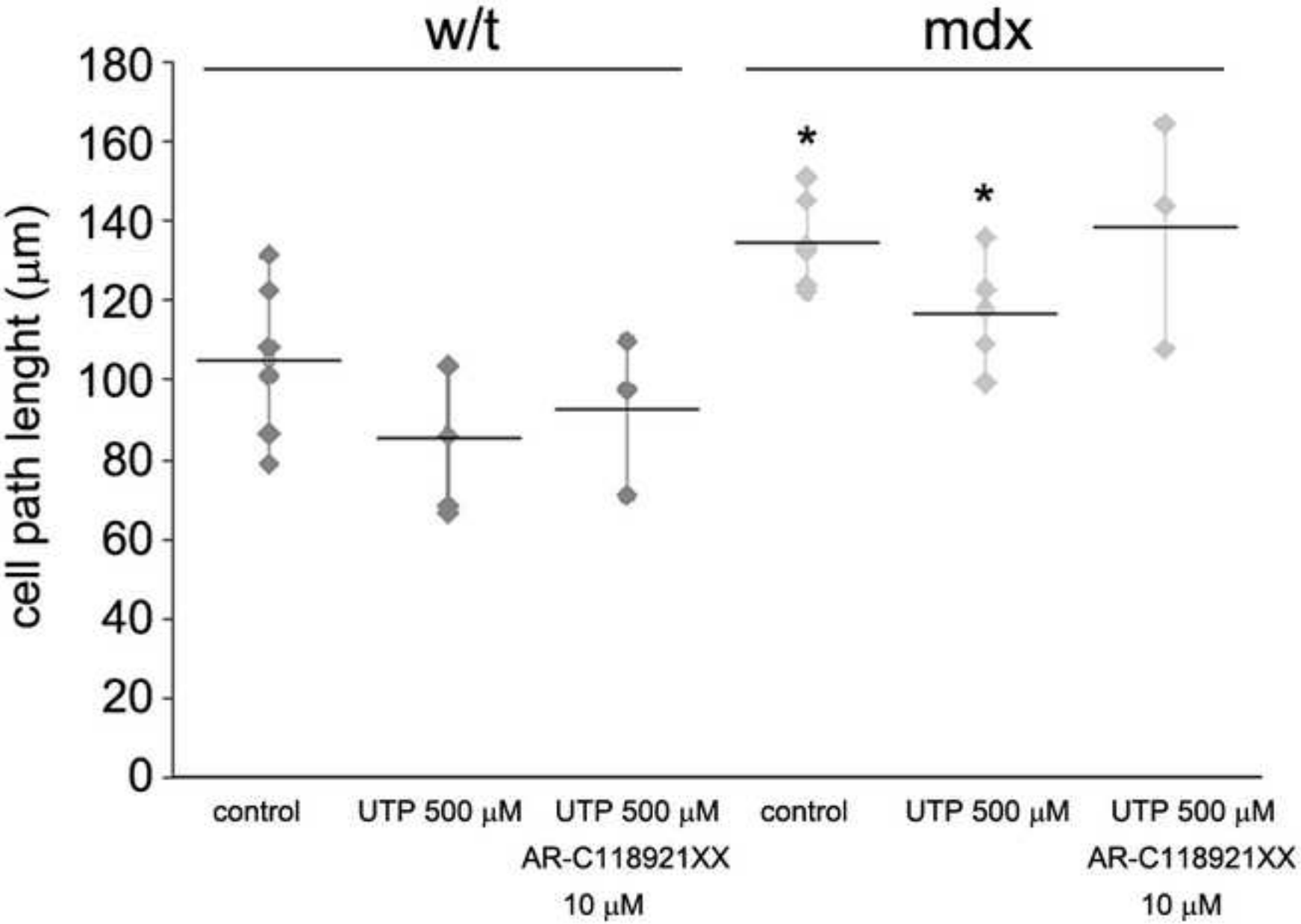
w/t
mdx
180
160
140
120
100
80
60
40
20
0
cell path lenght (µm)
*
*
control
UTP 500 µM
UTP 500 µM AR-C118921XX 10 µM
control
UTP 500 µM
UTP 500 µM AR-C118921XX 10 µM